Cite this: *Dalton Trans.*, 2022, **51**,  
1791

# Fluorescent organo-antimony compounds as precursors for syntheses of redox-active trimeric and dimeric alkali metal antimonides: an insight into electron transfer reduction processes†

Ekta Nag, <sup>a</sup> Aditya Kulkarni, <sup>a</sup> Sai Manoj N. V. T. Gorantla, <sup>b</sup> Nico Graw, <sup>c</sup> Maria Francis, <sup>a</sup> Regine Herbst-Irmer,<sup>c</sup> Dietmar Stalke, <sup>\*c</sup> Herbert W. Roesky, <sup>\*c</sup> Kartik Chandra Mondal <sup>\*b</sup> and Sudipta Roy <sup>\*a</sup>

(Tip)<sub>2</sub>SbCl (**1**, Tip = 2,4,6-triisopropylphenyl) has been utilized as a precursor for the synthesis of the distibane (Tip)<sub>4</sub>Sb<sub>2</sub> (**4**) via one-electron reduction using KC<sub>8</sub>. The two-electron reduction of **1** and **4** afforded the novel trinuclear antimonide cluster [K<sub>3</sub>((Tip)<sub>2</sub>Sb)<sub>3</sub>(THF)<sub>5</sub>] (**6**). Changing the reducing agent from KC<sub>8</sub> to a different alkali metal resulted in the solid-state isolation of corresponding stable dimeric alkali metal antimonides with the general formula [M<sub>2</sub>((Tip)<sub>2</sub>Sb)<sub>2</sub>(THF)<sub>p-x</sub>(tol)<sub>x</sub>] (M = Li (**14**), Na (**15**), Cs (**16**)). In this report, different aspects of the various reducing agents [K metal, KC<sub>8</sub>, and [K<sub>2</sub>(Naph)<sub>2</sub>(THF)]] used have been studied, correlating the experimental observations with previous reports. Additional reactivity studies involving **1** and AgNTf<sub>2</sub> (Tf = trifluoromethanesulfonyl) afforded the corresponding antimony cation (Tip)<sub>2</sub>Sb<sup>+</sup>NTf<sub>2</sub><sup>-</sup> (**19**). The Lewis acidic character of **19** has been unambiguously proved via treatment with Lewis bases to produce the corresponding adducts **20** and **21**. Interestingly, the precursors **1** and **4** have been observed to be highly luminescent, emitting green light under short-wavelength UV radiation. All the reported compounds have been characterized via NMR, UV-vis, mass spectrometry, and single-crystal X-ray diffraction analysis. Cyclic voltammetry (CV) studies of **1** in THF showed possible two electron reduction, suggesting the *in situ* generation of the corresponding radical-anion intermediate **1**<sup>-•</sup> and its subsequent conversion to the monomeric intermediate (Tip)<sub>2</sub>Sb<sup>-</sup> (**5**) upon further reduction. **5** undergoes oligomerization in the solid state to produce **6**. The existence of **1**<sup>-•</sup> was proved using electron paramagnetic resonance (EPR) spectroscopy in solution. CV studies of **6** suggested its potential application as a reducing agent, which was further proved via the conversion of Tip-PCl<sub>2</sub> to trimeric (Tip)<sub>3</sub>P<sub>3</sub> (**17**), and cAAC=P-Cl (cAAC = cyclic alkyl(amino)carbene) to (cAAC)<sub>2</sub>P<sub>2</sub> (**18**) and **4**, utilizing **6** as a stoichiometric reducing agent.

Received 8th October 2021,  
Accepted 21st December 2021

DOI: 10.1039/d1dt03398k

rsc.li/dalton

## Introduction

The transition of electrons (within a molecule or between two molecules) often leads to resultant electromagnetic radiation, which can be responsible for colourful sights around us. Electron transport (ET) (between molecules in solution or at a solid-solution interface) is one of the most important known processes in chemistry and bio-chemistry.<sup>1</sup> Controlled ET biochemical processes are fascinating and captivating. For example, proton pumping around the walls of mitochondria can happen due to a well-controlled ET process, finally enabling the reduction of molecular oxygen to water with release of energy.<sup>1b</sup> Fe-S-based electron transport proteins play a vital role in enabling the reduced form of the MoFe<sub>7</sub>S<sub>9</sub>C unit of the FeMoco enzyme to bind to molecular dinitrogen, followed by proton-coupled reduction to generate ammonia

<sup>a</sup>Department of Chemistry, Indian Institute of Science Education and Research (IISER) Tirupati, Tirupati 517507, India. E-mail: roy.sudipta@iisertirupati.ac.in

<sup>b</sup>Department of Chemistry, Indian Institute of Technology Madras, Chennai 600036, India

<sup>c</sup>Institut für Anorganische Chemie, Georg-August-Universität, Tammannstraße 4, 37077-Göttingen, Germany

† Electronic supplementary information (ESI) available: Experimental methods; syntheses of compounds **1**, **4**, **6**, and **14–21**; NMR spectra; UV-vis spectra; fluorescence data; single crystal X-ray diffraction data for **1**, **2**, **4**, **6**, and **14–21**; computational details; spectral data for compounds **1**, **4**, **6**, and **14–21**; copies of <sup>1</sup>H, <sup>13</sup>C, and <sup>15</sup>N NMR spectra; mass spectra (PDF). CCDC 2078143–2078148. For ESI and crystallographic data in CIF or other electronic format see DOI: 10.1039/d1dt03398k

under ambient conditions, which is one of the toughest tasks for chemists to achieve in the laboratory.<sup>2</sup>

In 1940, Marcus theory explained the thermodynamics and kinetics of ET processes.<sup>3</sup> According to this, outer sphere ET (Fig. S95A, ESI†) from one chemical species to a very close structural analogue will happen without significant structural changes (e.g., between  $\text{Fe}(\text{H}_2\text{O})_6^{2+}$  and  $\text{Fe}(\text{H}_2\text{O})_6^{3+}$  in water). The solvent molecules will remain in between these redox active species. The temperature and solvent polarity play important roles during this ET process. The solvent re-organization energy is related to the activation energy.<sup>4,5</sup> Finally, the existence of an inverted region relating to the kinetics was experimentally proven by Miller in 1980s.<sup>5a</sup> The classical and semi-classical quantum models of Marcus theory explain the slightly higher rate of reaction in the inverted region due to the overlap of vibrational energy levels of reactants and excited intermediates.<sup>5</sup> In contrast, the inner sphere mechanism (Fig. S95B, ESI†) involves changes in the primary coordination/solvent spheres of the reactants leading to the formation of intermediate exotic species *via* a bridging atom/group, which is broken after the ET process is complete.<sup>3</sup> Moreover, Marcus theory has been extended to address heterogeneous ET processes.<sup>6</sup> The formation of an electrical double layer and its effects have been addressed subsequently.<sup>7</sup>

Over the past two decades, electron-donating reducing agents, e.g., alkali metals ( $M = \text{Li}, \text{Na}, \text{K}, \text{Cs}$ ), their corresponding graphite intercalated compounds (GICs:  $\text{KC}_8, \text{KC}_{24}, \text{LiC}_6$ ), and alkali-metal naphthalenides ( $\text{MC}_{10}\text{H}_8$ ;  $M = \text{Li}, \text{Na}, \text{K}, \text{Cs}$ ), have been widely applied in synthetic organic<sup>8</sup> and inorganic/organometallic chemistry.<sup>9</sup> In particular, the employment of  $\text{Li}, \text{Na}, \text{K}, \text{KC}_8, \text{NaC}_{10}\text{H}_8$ , and  $\text{KC}_{10}\text{H}_8$  has been fruitful.<sup>10</sup> Extremely electropositive and highly reducing potassium metal possesses a bcc structure (Fig. 1, top left) in the solid state with multi-centre electronic delocalization.<sup>11</sup> Molten K-metal can be reacted with graphite at 200–250 °C for 1–8 h to produce a type-I GIC intercalated compound ( $\text{KC}_8$ ). Cationic  $\text{K}^+$  ions are intercalated between anionic single layers of graphene in an alternating fashion (Fig. 1, right) with partially

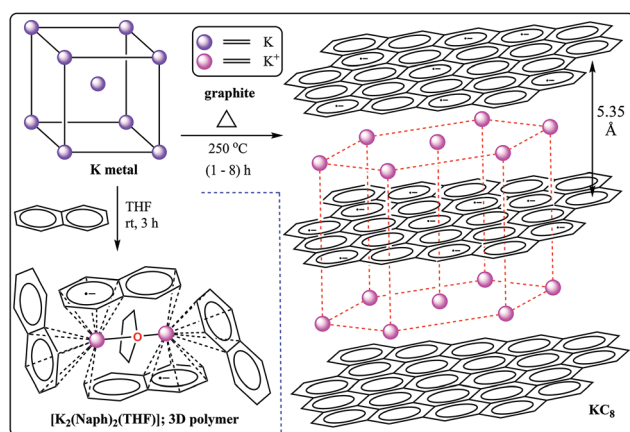


Fig. 1 The structure of K metal (bcc) and the syntheses and structures of potassium naphthalenide and  $\text{KC}_8$ .

filled  $\pi^*$  orbitals.<sup>12</sup> K metal is insoluble in organic solvents, while  $\text{KC}_8$  is sparingly soluble in DMSO at rt and in THF under high frequency ultrasonication.<sup>13</sup> Practically, at room temperature and without high-frequency sonication, graphite and  $\text{KC}_8$  are insoluble in THF, toluene, and *n*-hexane, which are most frequently utilized as reaction media; this is advantageous as they can be easily separated out of reaction mixtures *via* filtration.<sup>8,9</sup> However, the related ET reduction processes take place at the reaction solution/solid interface. Dark-green-coloured potassium naphthalenide,  $[\text{K}_2(\text{Naph})_2(\text{THF})]_n$ ,<sup>14</sup> is a soluble equivalent of golden-yellow-coloured  $\text{KC}_8$ .<sup>12</sup> In fact, the diluted/dispersed soluble form of  $\text{KC}_8$  in DMSO solvent is analogous to  $[\text{K}_2(\text{Naph})_2(\text{THF})]_n$ .<sup>13</sup> The naphthalenide ( $\text{Naph}^{\cdot-} = \text{C}_{10}\text{H}_8^{\cdot-}$ ) radical anion possesses an electron in a low-lying anti-bonding  $\pi^*$ -orbital which is easily oxidizable.<sup>14,15</sup> Some chemical reactions have been successfully carried out using  $[\text{K}_2(\text{Naph})_2(\text{THF})]_n$  in THF, while the same reactions have been unsuccessful when K metal or  $\text{KC}_8$  was employed as a reducing agent.<sup>16,17</sup> One example is the conversion of  $(\text{cAAC})\text{SiCl}_2\text{P-Tip}$  ( $\text{Tip} = 2,4,6\text{-triisopropylphenyl}$ ) to  $(\text{cAAC})\text{Si}=\text{P-Tip}$  and its dimeric form  $\{[(\text{cAAC})\text{Si-P-Tip}]_2\}$ .<sup>17</sup> In this present report, we shed light on the nature of ET processes based on structural properties of the reducing agents from the point of view of “Marcus” theory and some other recent scientific advancements. It is worth mentioning that in the past two decades, a few research groups have tried to explain how neutral monoatomic and diatomic Na metal and monoatomic  $\text{Na}^-$  anions are solvated in solution. These short-lived species ( $\text{Na}^0/\text{Na}_2^0/\text{Na}^-$ ) have been generated *via* the photolytic reduction of iodide anions.<sup>18</sup> The number of coordinated THF molecules varies depending on the oxidation state of Na. Coordinating THF molecules help  $\text{Na}^0/\text{Na}_2^0/\text{Na}^-$  to release their electrons *via* coulombic repulsion leading to the formation of higher-coordinated cations in solution.<sup>18</sup> The potential energies of the electrons of the outer shells of the reducing agents are quite high lying.<sup>12,14</sup> Contact electrification,<sup>19</sup> which is quite common, is an obvious way to transfer charge from an electron-rich centre to an electron-deficient centre at the surface. Anti-bonding electron jumping has been proposed as a mechanism involving absorbed species on a surface (Fig. 2).<sup>20,21</sup> In this context, the formation of an electrical double layer at the interface is the most obvious and crucial process.<sup>7</sup>

Organoantimony compounds have gained huge interest in recent times in materials research.<sup>22,23</sup> Antimony-based exotic radical cations, and anions have received significant scientific

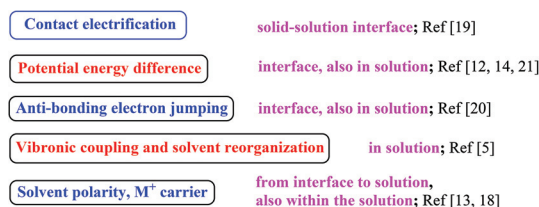


Fig. 2 Different aspects of ET processes at a solid-solution interface and in solution.

attention.<sup>24</sup> Some of these species are known to readily capture anions (e.g., F<sup>-</sup>)<sup>25</sup> to form higher-coordinated anions (e.g., SbF<sub>6</sub><sup>-</sup>) showing excellent fluorescence properties.<sup>26</sup> Considering the group 15 elements, as the atomic size increase down the group, the bond energy and nature of the bonds in tetra-substituted heavier homo-diatomic pnictogen compounds (Ar)<sub>4</sub>E<sub>2</sub> (E = P, As, Sb) vary substantially. Based on these factors, we envisioned that the reactivities of the neutral distibane (Tip)<sub>4</sub>Sb<sub>2</sub> and the corresponding anion and cation would be much different compared to the phosphorus analogs.<sup>27a</sup> Antimony-centred radicals are captivating.<sup>27b-e</sup> Herein, we report on the facile syntheses of the easily accessible green fluorescent chlorostibane (Tip)<sub>2</sub>SbCl (**1**) and the bulky Tip-group-stabilized distibane (Tip)<sub>4</sub>Sb<sub>2</sub> (**4**) (Tip = 2,4,6-triisopropylphenyl) as precursors for stabilizing the trinuclear antimonide cluster [K<sub>3</sub>((Tip)<sub>2</sub>Sb)<sub>3</sub>(THF)<sub>5</sub>] (**6**), the syntheses of three different dinuclear alkali metal antimonides with the general formula [M<sub>2</sub>((Tip)<sub>2</sub>Sb)<sub>2</sub>(THF)<sub>p-x</sub>(tol)<sub>x</sub>] (M = Li (**14**), Na (**15**), Cs (**16**)) using various reducing agents, and the rationalization of the respective ET processes. The precursors **1** and **4** and the complexes **6** and **14–16** have been studied *via* cyclic voltammetry (CV) in solution. In addition, the cationic antimony species (Tip)<sub>2</sub>Sb<sup>+</sup>NTf<sub>2</sub><sup>-</sup> (**19**) has been isolated and characterized, and the reactivity has also been studied. Moreover, the unusual chemical reactivity of the redox active trinuclear cluster **6** has been explored in solution.

## Results and discussion

Initially, the precursor chlorostibane (Tip)<sub>2</sub>SbCl (**1**) was synthesised *via* treating TipMgBr and SbCl<sub>3</sub> (1 : 1 molar ratio) in a mixture of solvents (THF/Et<sub>2</sub>O) from -78 °C to room temperature for 24 h. **1** was isolated as colorless rods/blocks in 73% yield after separating out the ionic byproduct [Mg<sub>2</sub>Cl<sub>3</sub>(THF)<sub>6</sub>][SbCl<sub>2</sub>Br<sub>2</sub>] (**2**) (see the ESI†). **1** has been well characterized based on NMR spectroscopy and X-ray single-crystal diffraction (see the ESI†). The ESI mass spectrum of THF solution of **1** (*m/z* = 561.2681, for the isotropic distribution see the ESI†) showed the existence of the de-halogenated cation (Tip)<sub>2</sub>Sb<sup>+</sup> (**1-Cl**)<sup>+</sup> (*m/z* = 527.2627, see the ESI†).

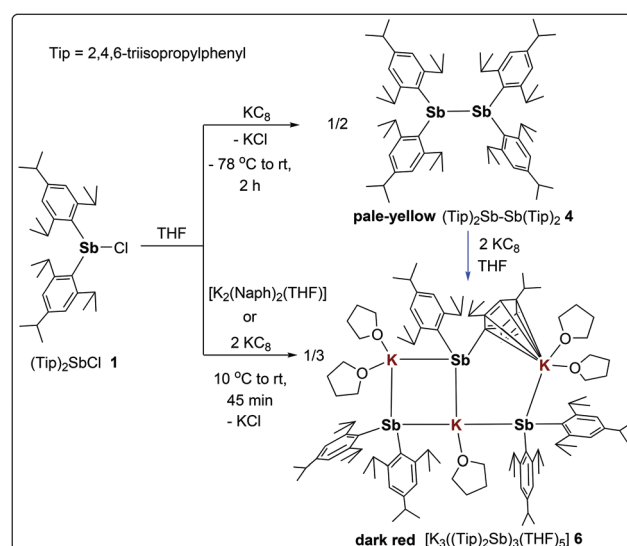
It is noteworthy to mention that although the reaction between SbCl<sub>3</sub> and TipMgBr was carried out at a 1 : 1 molar ratio, the expected product (Tip)<sub>2</sub>SbCl<sub>2</sub> could never be isolated. This observation can be rationalized based on the highly Lewis acidic nature of SbCl<sub>3</sub>, which can easily bind with bromide ions of TipMgBr in solution, leading to the formation of the crystalline colorless byproduct **2** in 97% yield (see the ESI†). **2** has been separated *via* filtration from a highly soluble THF/diethyl ether solution of compound **1**, and re-crystallized from highly concentrated diethyl ether solution as colorless blocks at room temperature and as rods from a freezer at -32 °C. In this context, it is noteworthy to mention that the previously reported phosphorus analogue ((Tip)<sub>2</sub>PCL) of **1** was prepared *via* reacting Tip-Li with PCl<sub>3</sub> under LiCl elimination.<sup>28</sup> On the contrary, previously reported<sup>27b</sup> (Tip)PCl<sub>2</sub> could be isolated in

high yield under identical synthetic conditions as described above at a 1 : 1 molar ratio of TipMgBr and PCl<sub>3</sub>, suggesting the significantly different reactivity of TipMgBr with PCl<sub>3</sub> and SbCl<sub>3</sub>. This can be attributed to the high anion binding affinity of SbCl<sub>3</sub>.

We have chosen three different reducing agents (Fig. 1), *i.e.*, K metal, KC<sub>8</sub>, and [K<sub>2</sub>(Naph)<sub>2</sub>(THF)], to study the modes of ET reduction processes, and to gain mechanistic insight.

The treatment of (Tip)<sub>2</sub>SbCl (**1**) with K metal in THF solvent led to the formation of a dark black insoluble precipitate which could not be characterized. A similar reaction, which was initiated with one equiv. of KC<sub>8</sub> in THF at -78 °C led to the formation of the light-yellow distibane (Tip)<sub>4</sub>Sb<sub>2</sub> (**4**) in 60% yield after stirring at rt for 2 h (Scheme 1). The yield of **4** was found to be quantitative when [K<sub>2</sub>(Naph)<sub>2</sub>(THF)] was employed as the reducing agent. Pale-yellow rods of **4** were grown from concentrated *n*-hexane or toluene solution from a freezer at -32 °C. The analogous compound (Tip)<sub>4</sub>P<sub>2</sub> was previously obtained *via* the reduction of (Tip)<sub>2</sub>PCL using Na or Mg metal in THF.<sup>27a</sup> The melting point range of **4** was found to be 95–96 °C. The ESI mass spectrum of THF solution of (Tip)<sub>4</sub>Sb<sub>2</sub> (**4**) showed *m/z* = 1056.5269 (see the ESI†) due to the formation of the monocation **4**<sup>+</sup> and the dication **4**<sup>2+</sup> (*m/z* = 527.2623, see the ESI†). The first and second ionization energies of (Tip)<sub>4</sub>Sb<sub>2</sub> (**4**) were theoretically computed to be 140.2 and 231.0 kcal mol<sup>-1</sup>, respectively.

Interestingly, the reduction of (Tip)<sub>2</sub>SbCl (**1**) with two equiv. of KC<sub>8</sub> in THF at 0–5 °C led to the immediate formation of a dark red color. The reaction mixture was stirred at room temperature for 45 min to obtain the novel trimeric solvent-truncated potassium antimonide [K<sub>3</sub>((Tip)<sub>2</sub>Sb)<sub>3</sub>(THF)<sub>5</sub>] (**6**) upon the elimination of KCl (Scheme 1). Graphite was separated out *via* filtration and the solvent was dried under vacuum, leading to the formation of a crystalline bright-red solid, which was then



**Scheme 1** The syntheses of the distibane (Tip)<sub>4</sub>Sb<sub>2</sub> (**4**) and trimeric potassium antimonide [K<sub>3</sub>((Tip)<sub>2</sub>Sb)<sub>3</sub>(THF)<sub>5</sub>] (**6**) from the precursor (Tip)<sub>2</sub>SbCl (**1**).

extracted with toluene. The conversion of **1** into **6** was found to be very fast when  $[K_2(\text{Naph})_2(\text{THF})]$  was utilized as the reducing agent. THF solution of **1** was cooled to  $-40\text{ }^\circ\text{C}$  and THF solution of  $[K_2(\text{Naph})_2(\text{THF})]$  was added dropwise to immediately obtain a dark red solution of **6**. The formation of a dark black solution with the deposition of black powder was observed when the reaction was carried out at  $5\text{ }^\circ\text{C}$ . Highly air- and moisture-sensitive dark-red plates of **6** were obtained in 59% and 95% yields using the two reducing agents,  $\text{KC}_8$  and  $[K_2(\text{Naph})_2(\text{THF})]$ , respectively, from concentrated toluene solution stored in a freezer at  $-32\text{ }^\circ\text{C}$ . **6** was found to be stable in solution and solid states under an argon atmosphere for more than six months and it decomposed to a black solid at  $130\text{ }^\circ\text{C}$ .

One- and two-electron reductions of **1** were carried out in THF.  $\text{KC}_8$  is insoluble and it can be dispersed at room temperature at low concentrations in THF.<sup>27c</sup> The ET process between  $(\text{Tip})_2\text{SbCl}$  (**1**) and  $\text{KC}_8$  occurs at the solution/solid interface ( $\text{KC}_8$ ; heterogeneous), while similar ET reduction between **1** and  $[K_2(\text{Naph})_2(\text{THF})]$  takes place in a homogeneous THF medium.<sup>14</sup> The ET reaction modes are illustrated in Fig. 3 and 5. Electron jumping is expected to take place to the  $\sigma^*_{\text{Sb-Cl}}$  bonds from the partially filled  $\pi^*$  orbitals of the anionic graphenide layers of  $\text{KC}_8$  (Fig. 1).<sup>12</sup> Subsequently,  $\text{K}^+$  ions can be transported to solution due to electrostatic interactions with the anions. Lone-pair-donating THF molecules<sup>18</sup> can coordinate with  $\text{K}^+$ , facilitating its migration from intercalated layers to solution. The formation of solvated tight ion pairs ( $\text{K}^+$ ,  $\text{e}^-$ ) has not yet been experimentally proven at the interface between THF solution and the solid surface of  $\text{KC}_8$ .<sup>18</sup> The diffusion of the  $(\text{Tip})_2\text{Sb}^\bullet$  radical,  $(\text{Tip})_2\text{SbCl}^{\bullet-}$  radical anion,  $(\text{Tip})_2\text{Sb}^-$  anion, or  $(\text{Tip})_2\text{Sb-K}(\text{THF})_n$  from the interface to bulk solution is controlled *via* magnetic stirring and the rate of electron jumping from the anionic graphenide layers is controlled *via* adjusting the temperature of the reaction solution (Scheme 2A).

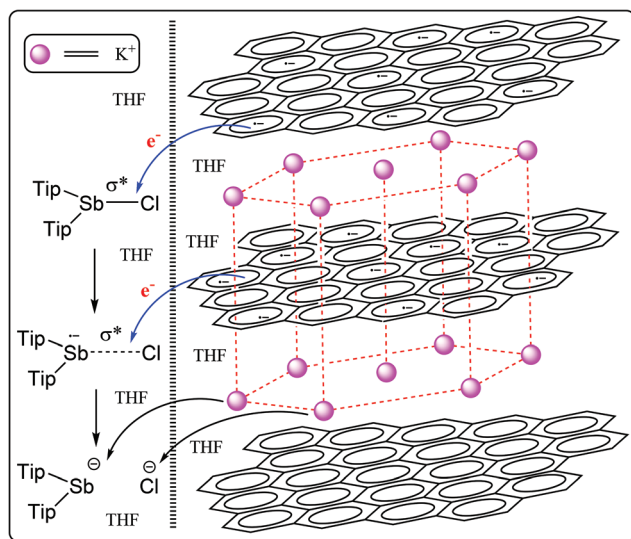
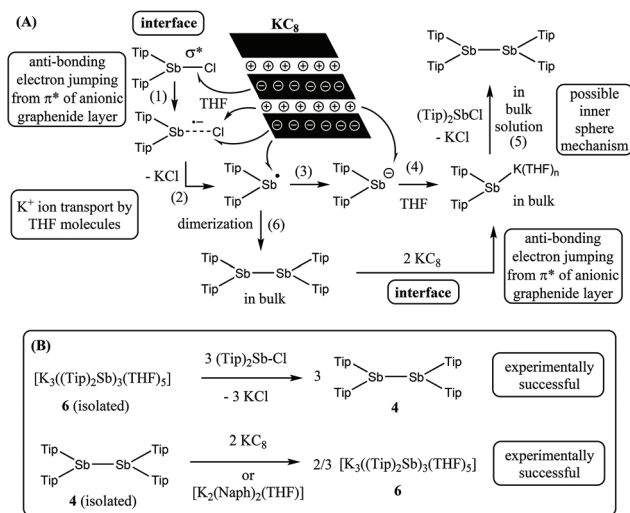


Fig. 3 The proposed electron transfer mode at the interface between solid  $\text{KC}_8$  and  $(\text{Tip})_2\text{SbCl}$  (**1**) in THF.



Scheme 2 The syntheses of the distibane  $(\text{Tip})_4\text{Sb}_2$  (**4**) and the trimeric potassium antimonide  $[K_3((\text{Tip})_2\text{Sb})_3(\text{THF})_3]$  (**6**) from the precursor  $(\text{Tip})_2\text{SbCl}$  (**1**).

The formation of the Sb-centered radical has been proved based on the observed EPR resonance at  $g = 2.12$  at room temperature (Fig. 4). Hyperfine lines for Sb [ $^{121}\text{Sb}$  (57.25%,  $I = 5/2$ ) and  $^{123}\text{Sb}$  (42.75%,  $I = 7/2$ )] are not clearly visible. A similar EPR spectrum for the stable  $\text{Sb}_2^{\bullet-}$  species has been reported at  $g = 2.16$ .<sup>24e</sup> That the radicals of group 15 elements have noticeably longer lifetimes has been recently summarized by Schulz *et al.*<sup>27c</sup> Because Sb is a heavy element, the separation between the nuclear spin energy levels and relaxation times of Sb are different, leading to a broad EPR signal.<sup>27b-e</sup> As a result, hyperfine lines are often not observed.<sup>24e,27c</sup>

Very recently ET from  $\text{KC}_8$  to Ph-CN ( $\pi^*$ ) has been shown *via* the formation of a  $\text{Ph-CN}^{\bullet-}$  radical anion, followed by the transport of a  $\text{K}^+$  ion to this anion.<sup>13a</sup> The formation of an electrical double layer<sup>7</sup> can be introduced at this interface, and the role of  $\text{K}^+$  ions can be rationalized.<sup>7</sup> Fine particles of  $\text{KC}_8$  can dissolve significantly in NMP and slightly in THF, while they can be significantly dispersed in DMSO, THF, and other cyclic ethers, which has been proven based on the light-scattering Tyndall effect.<sup>13b,c</sup>

The effects of temperature on the ET reduction process during the  $\text{KC}_8$ -mediated reduction of **1** at a 1:2 molar ratio

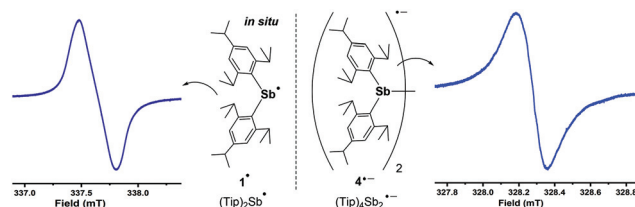
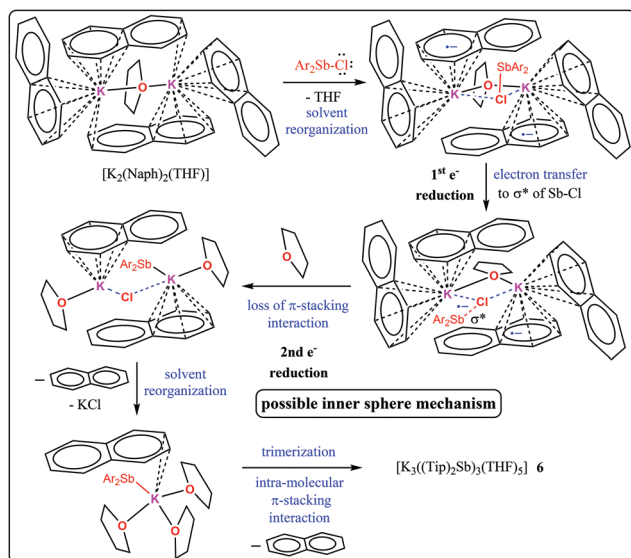


Fig. 4 X-band EPR spectra of a reaction mixture containing  $(\text{Tip})_2\text{SbCl}$  (**1**) and  $\text{KC}_8$  at a 1:2 molar ratio in THF at 293 K. Centre of signal = 3375 G,  $g = 2.12$  (left).<sup>24e</sup> The EPR resonance at a  $g$  value of around 2.0 suggests the presence of a C-centered radical intermediate in THF (right).

were studied. If the reaction between  $\text{KC}_8$  and **1** is initiated at a significantly lower temperature ( $-20\text{ }^\circ\text{C}$ ), the time for reaction completion becomes 4–5 times longer. Moreover, instead of the direct formation of a dark red solution of **6**, green solution is obtained initially, which slowly changes to light red and finally to dark brownish red. Attempts to isolate this green-coloured species remained unsuccessful, leading to the deposition of an insoluble black precipitate. This observation is similar to the case when **1** was reacted with K metal.

The ET reductions of  $(\text{Tip})_2\text{SbCl}$  (**1**) with  $[\text{K}_2(\text{Naph})_2(\text{THF})]$  in THF at 1:1 and 1:2 molar ratios proceed very smoothly with much higher yields (over 95%, confirmed *via* NMR measurements), leading to the isolation of **4** and **6**, respectively. These reactions should be initiated at least at  $-40\text{ }^\circ\text{C}$  with the dropwise addition of THF solution of  $[\text{K}_2(\text{Naph})_2(\text{THF})]$ . The reduction of **1** was expected to proceed *via* an inner sphere mechanism (Fig. 5), which might be the reason for the smooth reactions with high yields. In addition, **1** also reacts with **6** to produce **4** at a suitable molar ratio and, similarly, the latter can be converted to **6** and isolated in high yield (Scheme 2B; Fig. 6).

An identical reaction was carried out at  $-78\text{ }^\circ\text{C}$  to study the effects of the initial temperature on the reaction progress, and these conditions were found to be sluggish. Upon increasing the temperature from  $-78\text{ }^\circ\text{C}$  to room temperature, the color of the reaction mixture slowly turned from yellow to light green and then to dark green after stirring for another 5 h. The appearance of dark green color was assumed to be due to the formation of the radical anion  $[(\text{Tip})_2\text{Sb}-\text{Sb}(\text{Tip})_2]^-$  (**4**<sup>•-</sup>). However, the species **4**<sup>•-</sup> could not be isolated and characterized even after several attempts. In this context, it is important to mention that  $\text{Mes}_2\text{SbLi}$  and other metal antimonides reported so far were prepared *via* the deprotonation of  $\text{R}_2\text{SbH}$



**Fig. 5** The proposed ET reduction pathway in the chemical reaction between  $[\text{K}_2(\text{Naph})_2(\text{THF})]$  and  $(\text{Tip})_2\text{SbCl}$  (**1**) in solution (an inner sphere mechanism).

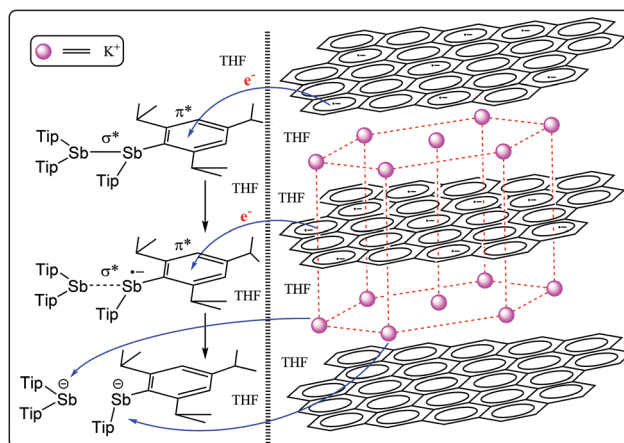


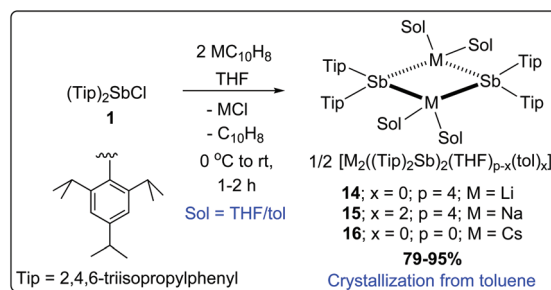
**Fig. 6** The proposed electron transfer mode at the interface of solid  $\text{KC}_8$  and  $(\text{Tip})_2\text{SbCl}$  (**1**) in THF. EPR resonance at a  $g$  value of around 2.0 suggests the formation of a C-centered radical intermediate in THF.

with  $\text{BuLi}$ .  $\text{R}_2\text{SbLi}$  ( $\text{R} = \text{Ph}, \text{Mes}$ ) was characterized in the solid state as monomeric  $\text{Li}(\text{Mes})_2\text{Sb}(\text{THF})_3$ .<sup>29</sup>

An earlier reported potassium antimonide was isolated as an infinite chain when crystallized with a triple-nitrogen-donating amine ligand.  $\text{R}_2\text{SbK}$  was generated *via* the reduction of cyclic  $(\text{RSb})_n$  using K metal in THF with the deposition of Sb powder ( $\text{R} = \text{Mes}$ ).<sup>29</sup>

Interestingly, the reduction of  $(\text{Tip})_2\text{SbCl}$  (**1**) in THF at  $0\text{ }^\circ\text{C}$  to room temperature in the presence of various freshly prepared dark green THF solutions of alkali-metal naphthalenides ( $\text{MC}_{10}\text{H}_8$ ,  $\text{M} = \text{Li}, \text{Na}, \text{Cs}$ ) afforded the corresponding dark-red dimeric alkali metal antimonides with the general formula  $[\text{M}_2((\text{Tip})_2\text{Sb})_2(\text{THF})_{p-x}(\text{tol})_x]$  ( $\text{M} = \text{Li}$  (**14**),  $\text{Na}$  (**15**),  $\text{Cs}$  (**16**);  $\text{tol} = \text{toluene}$ ) (Scheme 3).

Single crystals were not formed when the concentrated THF solutions were stored in a freezer, possibly due to the very high solubilities of these complexes. However, the dark brownish-red crystalline solids, which were obtained after the evaporation of the mother liquor, were redissolved in toluene and stored at  $0\text{ }^\circ\text{C}$  to obtain red-orange blocks/needle-shaped crystals of **14–16** in excellent yields (79–95%, Scheme 3). The reaction was observed to be fastest for Cs-naphthalenide and slowest for Li-naphthalenide, which can be rationalized based



**Scheme 3** The syntheses of dimeric alkali-metal antimonides ( $\text{M} = \text{Li}, \text{Na}, \text{Cs}$ ).

on the accumulation of electron density in the  $\pi^*$  orbital of naphthalene, which is similarly observed for  $\text{KC}_8$  and  $\text{LiC}_6$ .<sup>12a</sup> All these complexes show a dark-red color in THF and an orange-red color in aromatic solvents such as toluene and benzene.

The dimeric Na-antimonide (**15**) decomposed when highly concentrated toluene solution was stored at room temperature for more than 2 days. A greenish-brown solution was obtained when orange crystals of **15** were dissolved in  $\text{C}_6\text{D}_6$ .

Toluene coordinated with the Na center of **15** was observed (*via* NMR studies) to dissociate upon raising the temperature from room temperature to 70 °C (see the ESI†). The color of this NMR solution was found to change from light greenish-brown to darker greenish-brown, which could be described as solvatochromism (see the ESI†). Oil-coated red rods of **14** were found to be stable in air for more than 10 min. Complexes **6** and **14–16** were found to absorb in the range of 290–400 nm (see the ESI†). CV measurements of red THF solution of **15** suggested that the monomeric unit  $(\text{Tip})_2\text{Sb}-\text{Na}$  readily undergoes oxidation above  $-1.77$  V followed by dimerization to produce the pale-yellow compound **4** (see the ESI†). Complexes **14–16** were studied *via* NMR spectroscopy and were found to have common structural features (see the ESI†). The  $^7\text{Li}$  chemical shift value of complex **14** in  $\text{THF}-\text{D}_8$  was observed to be  $-0.3$  ppm at room temperature.

To investigate the effects of various solvents on the structures of complexes **14–16**, several reactions have been performed. The corresponding alkali-metal naphthalenides  $\text{MC}_{10}\text{H}_8$  were not formed in *n*-hexane/toluene, even after prolonged stirring, and hence they were prepared in a minimum volume of THF. When freshly prepared THF solution (0.5 ml) of  $\text{MC}_{10}\text{H}_8$  (2.1 mmol) ( $\text{M} = \text{Li}, \text{Na}, \text{Cs}$ ) was added to pre-cooled pale-yellow toluene/*n*-hexane solution (5 ml) of  $(\text{Tip})_2\text{SbCl}$  (0.09 mmol), immediate changes in colour from dark green to yellowish orange (**14**) with  $\text{LiC}_{10}\text{H}_8$ , to yellowish green (**15**) with  $\text{NaC}_{10}\text{H}_8$ , and to dark red (**16**) in the case of  $\text{CsC}_{10}\text{H}_8$  were observed. After 1 h, the resultant reaction mixtures turned dark red in all cases. The dark-red to yellowish-green solids isolated after the evaporation of the respective solvents were characterized *via*  $^1\text{H}$  NMR spectroscopy, confirming the formation of the same complexes **14–16**, respectively.

The computed solvation energies of **14** ( $\text{Li}$ :  $-2.88$  and  $-4.47$   $\text{kcal mol}^{-1}$ ) and **15** ( $\text{Na}$ :  $-7.85$  and  $-5.9$   $\text{kcal mol}^{-1}$ ) in toluene and *n*-hexane, respectively, were found to be significantly exothermic (see the ESI†).

The molecular structure of **1** is given in the ESI†. As expected for a  $\text{Sb(III)}$  compound, the Sb centre in **1** adopts trigonal pyramidal geometry.

Due to steric demand, the angle between the two bulky organic substituents is less compressed compared to the angles between both the Sb–C and Sb–Cl bonds. The distibane **4** crystallizes in the space group  $P\bar{1}$  with two molecules of **4** and *n*-hexane in an asymmetric unit (Fig. 7).

Both antimony atoms in **4** show trigonal pyramidal geometry, which might indicate the presence of a stereochemically active lone pair on each  $\text{Sb(III)}$  centre. Along the Sb–Sb bond

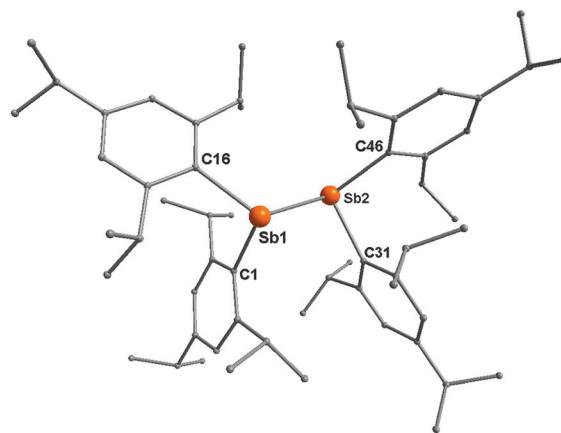
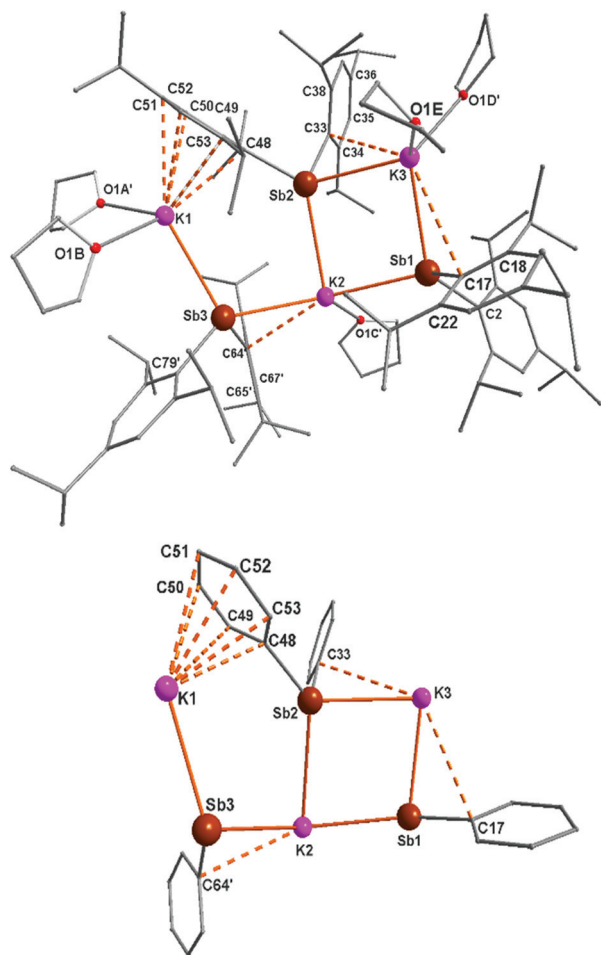


Fig. 7 The molecular structure of **4**. Hydrogen atoms and lattice solvent molecules are omitted for clarity. Selected experimental and calculated [at the M06-2X/B level of theory] bond lengths [Å] and angles [°]: Sb1–C1: 2.213(3), [2.207]; Sb1–C16: 2.207(3), [2.200]; Sb2–C31: 2.209(3), [2.209]; Sb2–C46: 2.209(3), [2.200]; Sb1–Sb2: 2.8587(6), [2.870]; C1–Sb1–C16: 95.89(13), [93.93]; C1–Sb1–Sb2: 91.27(9), [89.02]; C16–Sb1–Sb2: 112.52(9), [113.92]; C1–Sb1–Sb2–C31: 67.08(13), [64.38]; C16–Sb1–Sb2–C31: 163.99(13), [158.24].

axis, the molecule adopts a roughly staggered conformation with a torsion angle of about 164°. The Sb–Sb bond length is 2.86 Å in **4**, which is in the same range as observed for  $(\text{cAAC})_2\text{Sb}_2$  (2.81 Å)<sup>32</sup> and  $\text{Mes}_4\text{Sb}_2$  (2.85 Å;  $\text{Mes} = 2,4,6$ -trimethylphenyl)<sup>33</sup> and similar to the computed bond length of 2.87 Å (**4**). The C–Sb bond lengths in **4** lie in the range of 2.20–2.21 Å, which are comparable with those in  $(\text{Mes})_4\text{Sb}_2$  (2.20 Å)<sup>33</sup> and the computed C–Sb bond lengths of **4** (2.20–2.21 Å) but much longer when compared to  $\text{C}_{\text{cAAC}}\text{Sb}$  in  $\text{cAAC}_2\text{Sb}_2$  (2.08–2.09 Å).<sup>32</sup>

The molecular structure of the complex **6·1.5*n*-hexane** is shown in Fig. 8. It crystallizes in the monoclinic space group  $P2_1/c$ . Each Sb atom shows a distorted tetrahedral environment. As expected for a  $(\text{Tip})_2\text{Sb}^-$  fragment bearing two lone pairs, it adopts a bent structure with  $\text{C}_{\text{Tip}}\text{–Sb–C}_{\text{Tip}}$  angles ( $\sim 95^\circ$ ) smaller than  $109.5^\circ$ . Accordingly, the K1–Sb3–K2 angle is widened to about  $111^\circ$ . The  $\eta^6$  coordination of K1 to the aromatic ring system C48–C53 facilitates this widening as well. This cannot be observed for Sb1 and Sb2 due to the formation of a four-membered ring and the associated ring strain. All K ions in **6** are coordinated in distorted tetrahedral fashion. K1, K2, and K3 are bound to one, three, and two Sb atoms, respectively. K1 is located almost centrally, 2.927(2) Å above the aromatic system (C48–C53), clearly indicating cation– $\pi$  interaction. K2 and K3 show no comparable interactions, with the  $\text{K–C}_{\text{ipso}}$  distances ( $>3.4$  Å) being the shortest distances to any aromatic C atom. Additional coordination sites for all K atoms are occupied by THF solvent molecules. The C–Sb bond lengths fall in the range of 2.20–2.22 Å, showing little to no change when compared to the corresponding bond lengths in **4**. The distance from K2 to the nearest aromatic C atom is 3.41 (5) Å. The K–Sb distances fall in the range of 3.42 to 3.54 Å. The interactions between the aromatic ring and K1 centre are



**Fig. 8** The molecular structure of complex **6**-1.5*n*-hexane. Hydrogen atoms, lattice solvent, and disordered parts are omitted for clarity. Coordinating THF molecules and Tip substituents are shown in wire-frame format. Selected bond lengths [Å] and angles [°]: Sb1–C2: 2.197(2); Sb1–C17: 2.208(7); Sb2–C33: 2.210(2); Sb2–C48: 2.196(2); Sb3–C64: 2.217(7); Sb3–C79: 2.203(13); K1–Sb3: 3.5421(8); K2–Sb1: 3.4966(6); K2–Sb2: 3.5583(8); K2–Sb3: 3.4217(6); K3–Sb1: 3.4597(9); K3–Sb2: 3.5234(7); C(2)–Sb(1)–C(17): 95.2(3); C(79)–Sb(3)–C(64): 94.1(17); C33–Sb2–C48: 94.27(9); Sb1–K2–Sb2: 82.928(13); Sb1–K2–Sb3: 146.67(2); Sb2–K2–Sb3: 86.662(14); Sb1–K3–Sb2: 83.973(16); K2–Sb1–K3: 97.464(16); K2–Sb2–K3: 95.177(16); K1–Sb3–K2: 111.479(15).

significantly stronger than those involving the K2 and K3 centres, since K1 is bonded to only one Sb(Tip)<sub>2</sub> anion. The Sb2 and Sb3 centres of the Sb(Tip)<sub>2</sub> anions act as  $\mu$ -bridges between the two K ions (K2 and K3). The further growth of the ((Tip)<sub>2</sub>Sb–K)<sub>3</sub> unit in chain fashion is prevented due to coordination by THF molecules. The K–K and Sb–Sb distances are in the range of 5.22–5.75 Å and 4.67–4.79 Å, respectively. The K–Sb–K and Sb–K–Sb bridging angles are in the range of 95.177(16)–97.464(16)° and 82.928(13)–146.67(2)°, respectively.

Natural bond orbital (NBO) analysis (at the M06-2x/Def2-TZVPP level of theory) of complex **6** shows that molecular orbitals from HOMO to HOMO–2 represent lone pairs of electrons in p orbitals while molecular orbitals from HOMO–3 to

HOMO–5 represent lone pairs of electrons in s orbitals for the three Sb atoms. The molecular orbitals suggest that for Sb3, the lone pairs of electrons are oriented slightly away from the Sb3–K1 and Sb3–K2 bond axes (Fig. S45<sup>†</sup>), suggesting that these two bonds (Sb–K) are rather more ionic than covalent. NBO analysis shows that HOMO–302, HOMO–301, and HOMO–300 involve K $\cdots\pi_{\text{Tip}}$  interactions. HOMO–302 and HOMO–301 include the orbitals of K1, whereas HOMO–300 includes interactions between the orbitals of K2 and the  $\pi_{\text{Tip}}$  cloud (Fig. S55,† bottom). These interactions are found to be very weak, as the orbitals involved are extremely low lying (visualized with an isosurface value of 0.014–0.025). The results of NBO calculations show very small Wiberg bond indices of 0.05–0.07 for Sb–K bonds, correlating well with the positive total energy densities and low electron densities from quantum theory of atoms in molecules (QTAIM) analysis and suggesting Sb–K ionic interactions. No bond occupancies were observed for the Sb–K bonds (see the ESI<sup>†</sup>). The C–Sb–C angles in **6** vary in the range of 94.1–95.2°, which are close to 90°, suggesting the predominant participation of p orbitals in bonding, whereas in Mes<sub>2</sub>SbLi and Ph<sub>2</sub>SbLi, the C–Sb–C bond angles vary from 100.6–103.9°, which is closer to a tetrahedral angle.<sup>29</sup>

Single crystals of Li (**14**) and Na analogues (**15**) have been grown from toluene and characterized *via* X-ray single-crystal diffraction. The molecular structures of **14** and **15** are shown in Fig. 9. Both **14** and **15** crystallize in the space group *P*1̄. The (Tip)<sub>2</sub>Sb<sup>–</sup> anion acts as a  $\mu$ -bridge between the metal ions (Li/Na) (see the ESI<sup>†</sup>). The dimeric Li (**14**) and Na (**15**) complexes both possess a four-membered M<sub>2</sub>Sb<sub>2</sub> coplanar ring with M–Sb–M and Sb–M–Sb angles of 87.03(10)° (**14**)/91.38(4)° (**15**) and 92.97(10)° (**14**)/88.62(4)° (**15**), respectively. The C<sub>Tip</sub>–Sb–C<sub>Tip</sub> angles of **14** and **15** are similar to those of **6** (~95°).

Each Li ion of **14** is coordinated by two Sb atoms and two THF molecules, adopting distorted tetrahedral coordination geometry without any interaction between Li and the aromatic ring. In comparison, each Na ion of **15** is coordinated by two Sb atoms, one THF molecule, and one toluene molecule. The shortest Na–C<sub>toluene</sub> (Na1–C10A) distance is 3.014(5) Å (see the ESI<sup>†</sup> for all bond parameters).

Despite several attempts, single crystals of **16** suitable for single-crystal X-ray diffraction could not be obtained.

To gain insight into the electron transfer mechanism from KC<sub>8</sub> to (Tip)<sub>2</sub>SbCl (**1**) in solution, we performed cyclic voltammetry (CV) study of **1** in THF (Fig. 10 and the ESI<sup>†</sup>). The cyclic voltammogram of **1** showed a one-electron quasi-reversible (~200 mV) reduction at  $E_{1/2} = -1.15$  V, suggesting the formation of the corresponding radical anion [(Tip)<sub>2</sub>SbCl]<sup>•–</sup> (**1**<sup>•–</sup>) from the neutral molecule **1**.

To support the above experimental observations, we have also performed the geometry optimization of **1** at the M06-2X/B<sup>30</sup> level of theory. The energy gap between the HOMO (lone pair of electrons on Sb) and the LUMO ( $\sigma^*$  of Sb–Cl) for **1** was found to be 5.0 eV. Antimony inherently acts as a Lewis acid due to its electrophilic nature. The calculated gas phase electron affinity of **1** was found to be –30 kcal mol<sup>–1</sup>. NBO analysis at the M06/Def2-TZVPP level of theory revealed that the

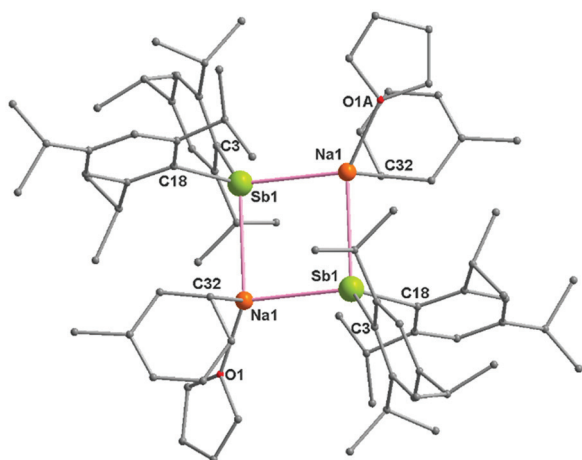
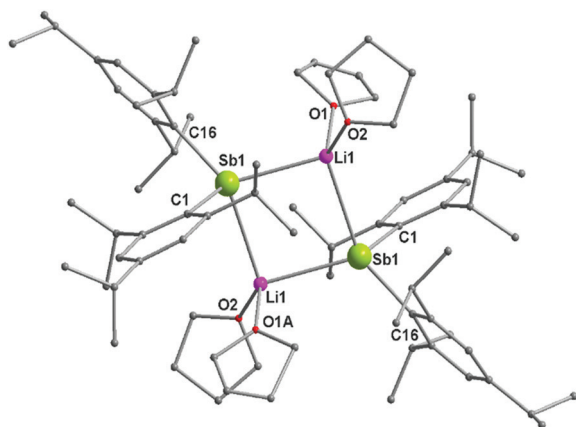


**Fig. 9** The molecular structures of dimers of (top)  $[\text{Li}_2((\text{Tip})_2\text{Sb})_2(\text{THF})_4]$  (**14**) and (bottom)  $[\text{Na}_2((\text{Tip})_2\text{Sb})_2(\text{THF})_2(\text{tol})_2]$  (**15**). For the sake of clarity, hydrogen atoms, lattice solvent, and disordered parts were omitted. In the cases of coordinating THF and Tip substituents, only the *ipso* atom is shown. Selected bond lengths (Å) and angles (deg.): **14**: Sb1–Li1: 2.916(4); Sb1–Li1A: 3.014(4); Li1–O1: 1.955(7); Li1–O2: 1.967(5); Sb1–C1: 2.193(2); Sb1–C16: 2.209(3); Li1–Sb1–Li1A: 87.03(10); Sb1–Li1–Sb1A: 92.97(10); C1–Sb1–C16: 95.1(2); C1–Sb1–Li1: 121.20(10); **15**: Sb1–Na1: 3.1564(16); Sb1–Na1A: 3.1579(15); Na1–O1: 2.281(9); Sb1–C1: 2.195(2); Sb1–C16: 2.197(2); Na1–Sb1–Na1A: 91.38(4); Sb1–Na1–Sb1A: 88.62(4); C1–Sb1–C16: 95.98(9); C1–Sb1–Na1 122.65(7).

LUMO of **1** is the  $\sigma^*$  orbital of the Sb–Cl bond, implying the *in situ* generation of the plausible radical anion intermediate  $1^{\cdot-}$  (Scheme 4).

Optimization of  $1^{\cdot-}$  revealed the cleavage of the Sb–Cl bond as indicated by the SOMO (equivalent to the LUMO ( $\sigma^*_{\text{Sb-Cl}}$ ) of  $1^{\cdot-}$ ) and the elongation of the Sb–Cl bond by  $\sim 0.69$  Å. This observation is also supported by a decrease in the Wiberg bond index (WBI) value of the Sb–Cl bond from 0.73 in **1** to 0.22 in  $1^{\cdot-}$  (see the ESI†).

The calculated spin density of  $1^{\cdot}$  on the Sb atom is 0.87 and the NPA charge on the Cl atom of  $1^{\cdot-}$  is  $-0.786e^-$ , which clearly indicates that  $1^{\cdot-}$  could undergo the elimination of the chloride ion to give the radical intermediate  $(\text{Tip})_2\text{Sb}^{\cdot}$  (**3**, Scheme 4). A concomitant increase in the spin density on Sb

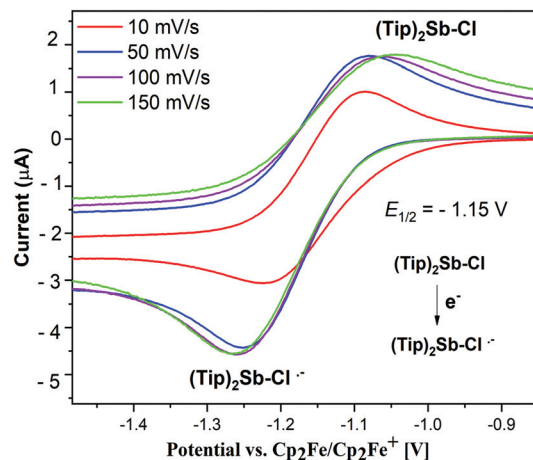
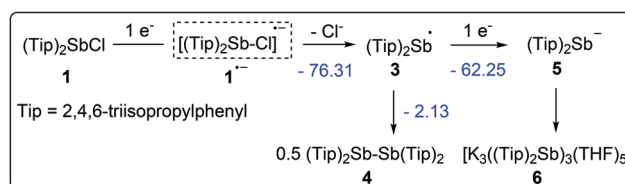


**Fig. 10** Cyclic voltammograms of THF solution of  $(\text{Tip})_2\text{SbCl}$  (**1**) with 0.1 M  $[n\text{-Bu}_4\text{N}]\text{PF}_6$  as the electrolyte at different scan rates (CE: Pt; WE: GC; RE: Ag).



**Scheme 4** The mechanism of the formation of **4** and **6** with computed  $\Delta G$  values in THF at 298.15 K in  $\text{kcal mol}^{-1}$ .

was observed from 0.87 in the case of  $1^{\cdot-}$  to 1.04 for **3**. Moreover, theoretical calculations showed that the generation of  $(\text{Tip})_2\text{Sb}^{\cdot}$  (**3**) from **1** is thermodynamically favourable (calculated  $\Delta G_{1\rightarrow 3} = -76.3$   $\text{kcal mol}^{-1}$ ). The Sb–Cl bond elongates from 2.406 Å in **1** to 3.096 Å in  $1^{\cdot-}$ . The radical spin density is mostly localized on Sb and Cl atoms, while a very small amount of electron density is found on the aromatic rings of the Tip group. This clarifies that electron transfer does not take place from  $\text{KC}_8$  to  $\pi^*$  of the Tip groups, but rather it occurs from  $\text{KC}_8$  to  $\sigma^*_{\text{Sb-Cl}}$  of **1** (see the ESI†).

The calculated C–Sb–C bond angle changes from  $94.4^\circ$  in **1** to  $96.7^\circ$  in  $1^{\cdot-}$ , rationalizing the easy cleavage of the Sb–Cl  $\sigma$ -bond of **1** upon reduction upon the elimination of KCl (Fig. 3 and 11, Scheme 4). The CV of **1** also showed an irreversible second electron transfer step corresponding to the formation of the monomeric anion  $(\text{Tip})_2\text{Sb}^{\cdot-}$  (**5**) from  $(\text{Tip})_2\text{Sb}^{\cdot}$  (**3**) ( $\Delta G^{298\text{K}} = -62.25$   $\text{kcal mol}^{-1}$ ), which occurs below  $-1.75$  V (see the ESI†). The intermediate **5** then undergoes oligomerization in the solid state to produce **6** (Scheme 4).

The aforementioned experimental data along with the theoretical calculations support the generation of the radical species  $(\text{Tip})_2\text{Sb}^{\cdot}$  (**3**) from **1** ( $\Delta G^{298\text{K}} = -2.13$   $\text{kcal mol}^{-1}$ ) via the intermediate  $1^{\cdot-}$ . The former can undergo further transformation via two competitive reaction pathways, *i.e.*, dimerization to produce **4** or further electron-mediated reduction to form **5**. The singlet state of **5** is calculated to be more stable by

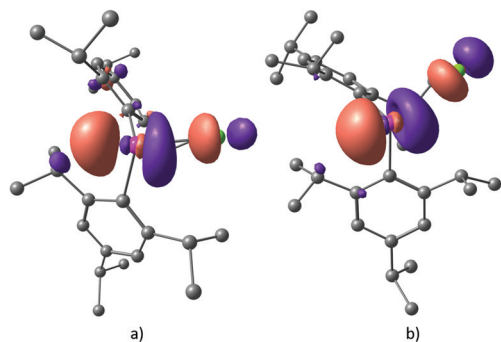


Fig. 11 (a) The LUMO of  $(\text{Tip})_2\text{SbCl}$  (**1**). (b) The SOMO of  $1^-$ .

32 kcal mol<sup>-1</sup> than the corresponding triplet state (see the ESI†). NBO analysis shows that one pair of electrons of the Sb atom in **5** is accommodated in the p orbital (HOMO) of the Sb atom and another lone pair of electrons is in the s orbital (HOMO-1) of the Sb atom of **5**.

The Sb-Sb bond in **4** has a WBI value of 0.88, confirming the presence of a single bond due to pure p-orbital overlap (HOMO).  $(\text{Tip})_4\text{Sb}_2$  (**4**) was indeed experimentally converted to  $[\text{K}_3((\text{Tip})_2\text{Sb})_3(\text{THF})_5]$  (**6**) when THF solution of  $(\text{Tip})_4\text{Sb}_2$  (**4**) was treated with two equiv. of  $\text{KC}_8$  at room temperature. This process was found to be quite facile and fast. Fig. 12 shows the CV diagram of **4** in THF, suggesting irreversible one-electron reduction.

Indeed, we see the reduction of **4** when treated with 2 equiv. of  $\text{KC}_8$  to produce **6** (Scheme 2, Fig. 6). On the contrary, Pan *et al.* showed that the P analog of **4**  $(\text{Tip})_4\text{P}_2$  undergoes one-electron oxidation to give the corresponding radical cation and di-cation based on cyclic voltammetry studies.<sup>27</sup> CV studies of the previously reported species  $((\text{TMS})_2\text{CH})_2\text{Sb}_2$  shows a  $E_{1/2}$  value of -1.65 V in THF<sup>27b</sup> which is in between

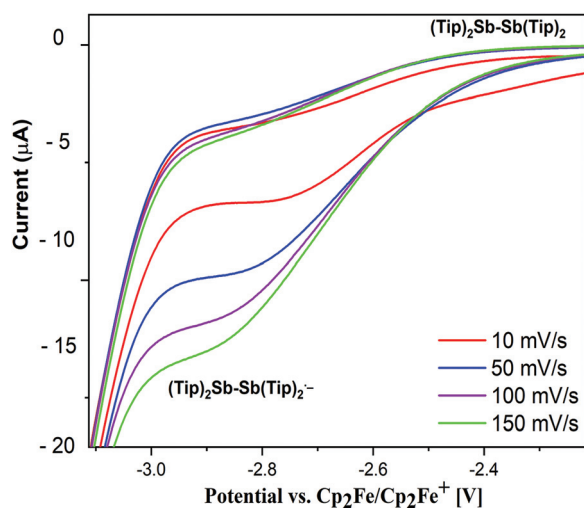
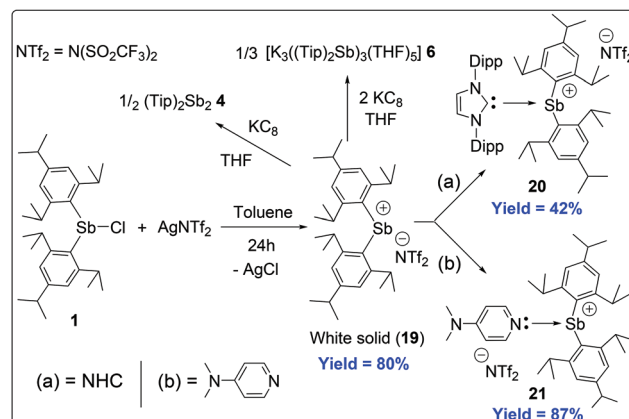


Fig. 12 Cyclic voltammograms of THF solution of  $\text{Tip}_4\text{Sb}_2$  (**4**) with 0.1 M  $[\text{n-Bu}_4\text{N}]\text{PF}_6$  as the electrolyte at different scan rates (CE: Pt; WE: GC; RE: Ag).

the  $E_{1/2}$  values of  $(\text{Tip})_2\text{SbCl}$  (**1**) and  $(\text{Tip})_2\text{Sb}_2$  (**4**). The UV-vis band of the reported  $((\text{TMS})_2\text{CH})_2\text{Sb}_2^{\cdot-}$  radical anion is observed at 812 nm ( $\pi \rightarrow \pi^*$ ). The EPR spectrum of the corresponding radical species is reported to be very broad and does not produce any experimental hyperfine coupling constant value.<sup>27b</sup>

As evidenced by the ESI mass spectrometric analysis of **1**, we observed the existence of the de-halogenated cation  $(\text{Tip})_2\text{Sb}^+$  (**1-Cl**)<sup>+</sup>. In order to attempt the synthesis of  $(\text{1-Cl})^+$ , we first calculated the bond dissociation energy of Sb-Cl in **1**, which is 64.7 kcal mol<sup>-1</sup> [ $(\text{Tip})_2\text{SbCl}(\text{g}) \rightarrow (\text{Tip})_2\text{Sb}^+(\text{g}) + \text{Cl}^-(\text{g})$ ]. The calculated C-Sb-C bond angle changes from 94.4° in **1** to 100.8° in the cation  $(\text{1-Cl})^+$ , which was found to be largely stabilized by the delocalization of the lone pair of electrons on the Sb atom over both the adjacent aromatic rings of the Tip group (see the ESI†). The extent of the electronic delocalization is significantly higher in the cation  $(\text{1-Cl})^+$  than in neutral compound **1** (see the ESI†). The formation of the cation  $(\text{1-Cl})^+$  is not facile under normal conditions due to the polar-covalent nature of the Sb-Cl bond. However, theoretical calculations showed that the HOMO-LUMO energy gap is reduced by 1.75 kcal mol<sup>-1</sup> upon the formation of the cation  $(\text{1-Cl})^+$ . Hence, the electronic reduction of the cation is predicted to be more facile if generated in solution.

To our delight, the cation  $(\text{1-Cl})^+$  was indeed experimentally generated in toluene when  $(\text{Tip})_2\text{SbCl}$  (**1**) was reacted with  $\text{AgNTf}_2$  at a 1 : 1 molar ratio (see the ESI†). The formation of the cation  $(\text{Tip})_2\text{Sb}^+\text{NTf}_2^-$  (**19**) was confirmed *via* NMR and ESI mass spectrometric analysis (see the ESI†). The Lewis acidic character of **19** was confirmed through its reaction with Lewis bases, *e.g.*, N-heterocyclic carbene (<sup>i</sup>PrNHC) and 2,2-dimethylaminopyridine (DMAP), resulting in the isolation of the corresponding adducts **20** (42%) and **21** (87%), respectively, in moderate to good yields (Scheme 5). Both adducts were characterized *via* NMR spectroscopy. The more upfield-shifted (2.35 ppm) isopropyl protons of the Tip and Dipp (2,6-diisopropylphenyl) groups in the <sup>1</sup>H NMR spectrum of **20** when compared with cation **19** (3.47 and 2.68 ppm) indicated the



Scheme 5 The reactivity of the cation  $(\text{Tip})_2\text{Sb}^+\text{NTf}_2^-$  (**19**) with Lewis bases and its reduction.

greater electron density at the adjacent Sb centre upon adduct formation. In addition, an upfield shift was also observed in the  $^1\text{H}$ - $^{15}\text{N}$  HMBC spectrum of the adduct **20** [ $^{15}\text{N}$  ( $\delta$ ): -196.85 ppm] compared to that of NHC [ $^{15}\text{N}$  ( $\delta$ ): -185.1 ppm], which is due to the possible conjugation of the double bond present at the five-membered backbone of NHC with the N atoms adjacent to  $\text{C}_{\text{carbene}}$ .<sup>31</sup> We have also optimized the geometry and performed NBO analysis of the cation  $(\text{Tip})_2\text{Sb}^+$  at the M06-2X/Def2-TZVPP level to study the nature of bonding, the charge distribution, and the electronic structure (see the ESI†). The NBO analysis showed that the LUMO is the vacant  $\sigma^*$  orbital of Sb and the HOMO consists of the lone pair on the Sb atom. The electron density in HOMO-1, HOMO-2, and HOMO-3 is located on the Tip group.

In an effort to synthesize Lewis acid/base adducts with  $(\text{Tip})_2\text{SbCl}$ , we have treated the Lewis-acidic cation  $[(\text{Tip})_2\text{Sb}]^+[\text{NTf}_2]^-$  (**19**) with NHC and DIMAP (dimethylaminopyridine). The formation of the respective adducts (**20** and **21**) with these two donor base ligands was confirmed based on  $^1\text{H}$  and  $^{13}\text{C}$  NMR spectra. In the  $^{13}\text{C}$  NMR spectrum, resonance due to  $\text{C}_{\text{NHC}}$  at 184.3 ppm (**20**) was observed, which is shifted upfield when compared to corresponding free  $\text{C}_{\text{NHC}}$  (220 ppm).

Bertrand *et al.* reported the cyclic alkyl(amino) carbene (cAAC) adduct  $\text{cAAC}^{\text{Cy}}\text{SbCl}_3$  with a  $\text{C}_{\text{cAAC}}$  resonance at 228.4 ppm.<sup>34</sup> Goicoechea and co-workers reported the Lewis acid-base adduct  $[\text{Dipp}_2\text{Im}\text{-SbBr}_2][\text{AlBr}_4]$ (1,3-bis(2,6-diisopropylphenyl)-imidazol-2-ylidene) of  $\text{SbX}_3$  (X = Br, F) with NHC through halide abstraction, where  $\text{C}_{\text{carbene}}$  appears at 150.3 ppm.<sup>35</sup> Recently, Gilliard and coworkers reported the NHC adduct of the antimony compound  $(\text{NHC})\text{-SbPh}_2\text{Cl}$ , where the  $\text{C}_{\text{carbene}}$  signal appears at 146.5 ppm.<sup>36</sup> The same group also reported carbene- and carbene-stabilized bismuth mono-, di-, and tri-cations.<sup>37</sup> The NHC- and cAAC-supported bismuth cations were prepared *via* directly treating the more sterically crowded carbene ligands with  $[\text{Ph}_2\text{Bi}(\mu\text{-Cl})_2]$ . The NHC-supported bismuth cation  $[(\text{SIPr})\text{BiPh}_2][\text{Ph}_2\text{BiCl}_2]$ (1,3-bis(2,6-diisopropylphenyl)imidazolidene) and cAAC-supported  $[(\text{cAAC})\text{BiPh}_2][\text{Ph}_2\text{BiCl}_2]$  showed carbene carbon resonances at 199.3 and 244.9 ppm, respectively. There are several other reports on antimony cations.<sup>38-40</sup>

### Reactivity of complex 6

Before investigating its reactivity, THF solution of **6** was studied *via* CV, and it showed one-electron quasi-reversible ( $\sim 250$  mV) oxidation at  $E_{1/2} = -2.25$  V, suggesting the formation of a radical intermediate  $(\text{Tip})_2\text{Sb}^{\cdot}$  (**3**) and the possible donation of an electron from **6** to a suitable acceptor (Fig. 13).

Following this cyclic voltammetry study, when  $[\text{K}_3((\text{Tip})_2\text{Sb})_3(\text{THF})_5]$  (**6**) was treated with an equimolar mixture of  $\text{Tip-PCl}_2$  in THF at room temperature, we observed the formation of the cyclic trimer  $(\text{Tip})_3\text{P}_3$  (**17**), which was further characterized *via* NMR spectroscopy (see the ESI†).<sup>28</sup> Further, we attempted to synthesize the heteronuclear diatomic species  $(\text{cAAC})\text{P-Sb}(\text{Tip})_2$  (**18**) *via* reacting **6** with cyclic alkyl(amino)carbene (cAAC)-stabilized chloro-phosphinidene,

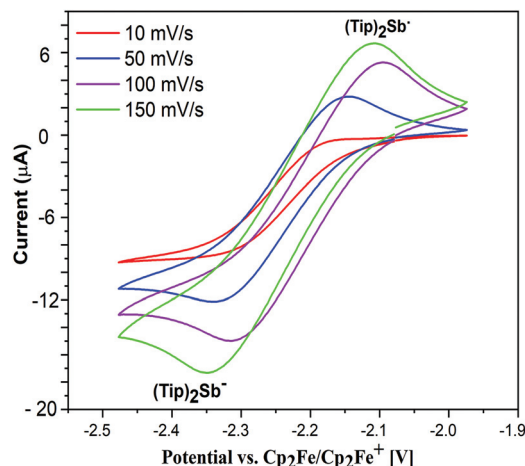
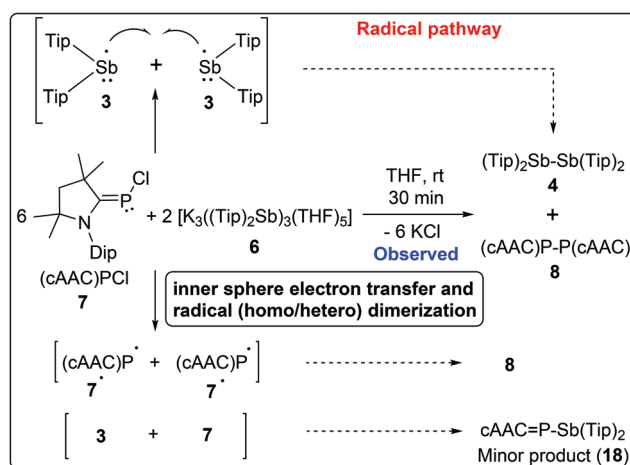


Fig. 13 Cyclic voltammograms of THF solution of  $[\text{K}_3((\text{Tip})_2\text{Sb})_3(\text{THF})_5]$  (**6**) with 0.1 M  $[\text{n-Bu}_4\text{N}]\text{PF}_6$  as the electrolyte at different scan rates (CE: Pt; WE: GC; RE: Ag).



Scheme 6 The reduction of  $\text{cAAC}=\text{P}-\text{Cl}$  (**7**) with compound **6** to generate  $\text{cAAC}_2\text{P}_2$  (**8**).

$\text{cAAC}=\text{P}-\text{Cl}$  (**7**). However, NMR studies revealed the formation of  $(\text{cAAC})_2\text{P}_2$  (**8**)<sup>41</sup> and  $(\text{Tip})_4\text{Sb}_2$  (**4**) as major products, with the formation of **18** only as a minor product; these were isolated experimentally and characterized *via* NMR (Scheme 6 and the ESI†). This type of chemical reaction has not reported thus far with analogous  $\text{R}_2\text{P}^-$  anions. Previously,  $(\text{Tip})_3\text{Sb}^{++}$  was shown to react with 1,4-benzodiquinone.<sup>24c</sup>

### Photophysical properties

All the Sb compounds (**1**, **4**, **6**, and **14-16**) have been characterized *via* UV/vis and fluorescence<sup>25,26</sup> measurements (see the ESI† for details). Compounds **1** and **4** have been found to be significantly fluorescent. Compound **1** has been found to be more fluorescent than **4**, due to the orbital mixing of Sb and Cl atoms, which has been seen in NBO analysis.

UV-vis bands for compounds **1** and **4** have been observed in the range of 290–400 nm (see the ESI†). Excitation in the range

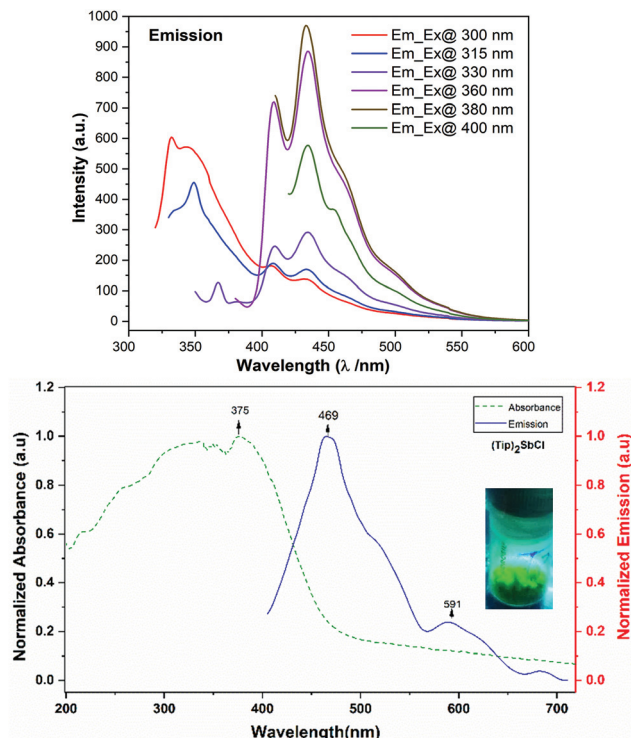


Fig. 14 Emission spectra of  $(\text{Tip})_2\text{SbCl}$  (**1**) in toluene (top) and in the solid state (bottom).

of 300–380 nm led to emission in the range of 400–500 nm (Fig. 14). The solid-state absorption of **1** at 375 nm resulted in emission at 469 and 591 nm, which explains the green emission under UV light.

The average lifetime of **1** in toluene has been calculated to be 2.3 ns under excitation of 433 nm with a quantum yield ( $\phi$ ) of 1.1% (see the ESI<sup>†</sup> for details).

### Theoretical studies

From TD-DFT calculations of **1**, we have observed that the electron density in the HOMO representing the lone pair of electrons on Sb and its delocalization on the aromatic ligand of neutral **1** is excited to the LUMO representing the vacant p orbital of **1** (Fig. 15, top) under excitation. We have optimized the singlet biradical state (**1\***) of  $(\text{Tip})_2\text{SbCl}$  (**1**) at the UM062x/Def2-TZVPP level. The biradical is delocalized on the aromatic ring and central Sb atom (Fig. 15, bottom). Upon exciting neutral  $(\text{Tip})_2\text{SbCl}$  (**1**), the lone pair on Sb gets excited to the excited singlet state, eventually coming back to the ground state *via* radiative decay. The singlet biradical state is 4.25 eV (98 kcal mol<sup>-1</sup>) higher in energy than the closed shell singlet ground state. This energy difference closely matches the energy of a photon (300 nm, see the ESI<sup>†</sup>) required to excite **1** → **1\*** (Fig. 15).

The light-yellow compound  $(\text{Tip})_4\text{Sb}_2$  (**4**) with a Sb–Sb bond length of 2.8587(6) Å can form its radical anion intermediate  $4^{\cdot-}$  (calculated Sb–Sb distances of 2.840/3.596 Å for  $(\text{Mes})_4\text{Sb}_2/\text{Mes}_4\text{Sb}_2^{\cdot-}$ , see the ESI<sup>†</sup>), which has been studied *via* theoret-

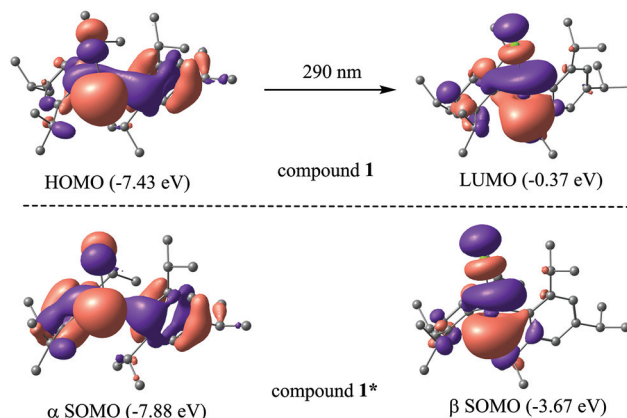


Fig. 15 (Top) The transition from the HOMO to the LUMO of **1** (from TD-DFT calculations at the M062x/Def2-TZVPP level) and (bottom) the  $\alpha$ - and  $\beta$  SOMOs of the excited singlet biradical state (**1\***) at the UM062x/Def2-TZVPP level of theory.

tical calculations and CV (for CV studies of **4** see Fig. 12 and the ESI<sup>†</sup>).

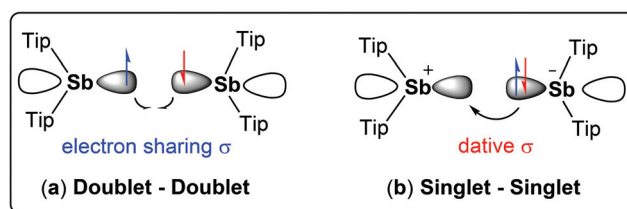
The optimization of  $\text{Tip}_4\text{Sb}_2$  as a dianion *via* adding another electron to  $4^{\cdot-}$  leads to the cleavage of the Sb–Sb bond forming the  $(\text{Tip})_2\text{Sb}^-$  anion (**5**). Experimentally we have observed that upon treatment with  $\text{KC}_8$ , neutral  $(\text{Tip})_4\text{Sb}_2$  yields the dark-red coloured anion **6** in THF solution (see the ESI<sup>†</sup>).

### EDA-NOCV analysis

To understand the reactivity and electron-mediated cleavage of the Sb–Sb bond of **4**, we have performed energy decomposition analysis coupled with natural orbital for chemical valence (EDA-NOCV).

We have considered two different bonding possibilities *via* varying the charge and electronic states of interacting fragments to give the best bonding description of the Sb–Sb bond of **4**: (a) neutral  $(\text{Tip})_2\text{Sb}$  fragments in an electronic doublet state forming an electron-sharing  $\sigma$  bond and (b) singly charged  $(\text{Tip})_2\text{Sb}^+$  and  $(\text{Tip})_2\text{Sb}^-$  fragments in an electronic singlet state coupling to form a dative  $\sigma$  bond (Scheme 7).

The bonding possibility with the lowest  $\Delta E_{\text{orb}}$  value is considered to be the best bonding representation, since it needs the least change in the electronic charge of the fragments to make the electronic structure of the species.<sup>24d</sup> The bonding



Scheme 7 The bonding possibilities in the  $(\text{Tip})_4\text{Sb}_2$  (**4**) compound. The Sb–Sb bond of **4** possesses 6% s and 94% p character.

possibility represented in Scheme 7(a) demonstrates the interaction of neutral fragments in an electronic doublet state forming an electron-sharing  $\sigma$  bond, which is the best bonding description since it gives the lowest  $\Delta E_{\text{orb}}$ , provided by the breakdown of  $\Delta E_{\text{orb}}$  into pairwise contributions (see Table S5†). This agrees with NBO analysis, showing an Sb–Sb bond with equal contributions (50%) from each Sb atom of **4** with 6% s and 94% p character. The electrostatic contribution (43.5%) is slightly higher than the orbital contribution (37.1%) towards the total attractive interactions. Interestingly, dispersion interactions provide a significant contribution of 19.4% towards the total attractive interactions. The notable dispersion and electrostatic contributions can be attributed to the large electron clouds of heavy antimony atoms. The instantaneous interaction energy  $\Delta E_{\text{int}}$  denotes the strength of the bond; for the Sb–Sb bond this is predicted to be 65.4 kcal mol<sup>-1</sup>. The Pauli repulsion  $\Delta E_{\text{Pauli}}$  between the two Sb atoms is calculated to be 156.1 kcal mol<sup>-1</sup>, and this is compensated by collective attractive interactions. The domination of the electrostatic and dispersion contributions and the relatively low instantaneous interactions indicate the existence of a not-so-strong Sb–Sb bond which can be broken easily, inferring its reactivity. There are three relevant pairwise orbital contributions  $\Delta E_{\text{orb}(1)} - \Delta E_{\text{orb}(3)}$  corresponding to the total orbital interactions which can be visualized based on deformation densities and associated molecular orbitals (Fig. 16 and the ESI†).

The strongest example  $\Delta E_{\text{orb}(1)}$  represents the electron-sharing  $\sigma$ -interactions of unpaired electrons in the SUMO of (Tip)<sub>2</sub>Sb fragments, and it contributes 76.8% to the total orbital contributions. The contribution of  $\Delta E_{\text{orb}(2)}$  (4.6%) comes from polarization between the HOMOs of the (Tip)<sub>2</sub>Sb fragments, and charge transfer can be observed partly into the SOMO and slightly into the high-lying LUMO+15 of another (Tip)<sub>2</sub>Sb fragment. In contrast,  $\Delta E_{\text{orb}(3)}$  (3%) due to  $\pi$  donation from the HOMO–5 of one (Tip)<sub>2</sub>Sb fragment into the LUMO+2 of another (Tip)<sub>2</sub>Sb fragment is weaker than  $\Delta E_{\text{orb}(1)}$ .

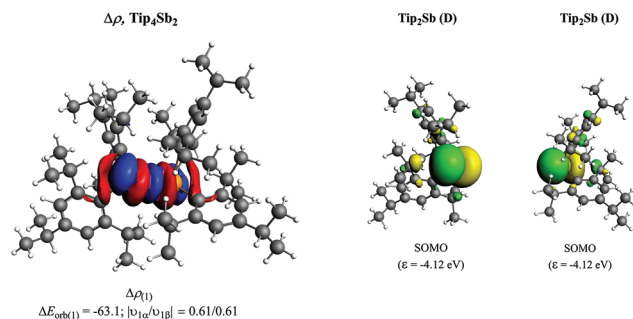


**Fig. 16** The shape of the deformation density  $\Delta\rho_{(1)}$  that corresponds to  $\Delta E_{\text{orb}(1)}$  and the associated MOs of (Tip)<sub>4</sub>Sb<sub>2</sub> (**4**), and the fragment orbitals of neutral (Tip)<sub>2</sub>Sb and (Tip)<sub>2</sub>Sb in the doublet state at the BP86–D3 (BJ)/TZ2P level. The iso-surface values are 0.001 a.u. for  $\Delta\rho_{(1)}$ . The eigenvalues  $|\nu_n|$  give the size of the charge migration in e. The direction of the charge flow of the deformation densities is from red to blue.

NBO and EDA-NOCV analyses on the nature of the Sb–Sb bond and its reactivity can be utilized to infer the formation of other antimonides starting from tetrameric cyclic R<sub>4</sub>Sb<sub>4</sub> precursors *via* alkali metal reduction in solution.<sup>29</sup> The significant contribution from the dispersion energy (19.4%) to the total stabilization energy of the Sb–Sb bond is found to be remarkable. The instantaneous interaction energy  $\Delta E_{\text{int}}$  of **4** is found to be 65.4 kcal mol<sup>-1</sup>. The interaction energy  $\Delta E_{\text{int}}$  of the Sb–Sb bond in Tip<sub>4</sub>Sb<sub>2</sub> (**4**) is relatively lower than that of the Sb–Sb bond in free Sb<sub>2</sub> (74.2 kcal mol<sup>-1</sup>). However, the strength of the Sb–Sb bond is significantly lower than that of lighter N–N (240.2 kcal mol<sup>-1</sup>) and P–P bonds (118.5 kcal mol<sup>-1</sup>).<sup>42,43</sup> Akin to a free Sb–Sb bond, electrostatic (coulombic) interactions dominate the total attractive interactions and  $\sigma$  contributions dominate the total orbital contributions. The natures of E–E bonds (E = group 15 element) in ligand-stabilized complexes are relatively unexplored to the best of our knowledge compared to group 13 and group 14 element stabilized complexes. The two Sb–C bonds of reported mono-cationic (cAAC)<sub>2</sub>Sb<sup>+</sup> species possess a dispersion energy of –30.2 kcal mol<sup>-1</sup>.<sup>24d</sup>

## Conclusions

To summarise, we have demonstrated a facile synthetic procedure to obtain green-light-emitting fluorescent diarylstibane-halide and distibane stabilized by bulky Tip groups. The ET reduction processes have been rationalized based on previous reports and correlated with our experimental observations. Such elaborations and illustrations of possible ET reduction processes are unprecedented in the area of main group chemistry. Different levels of quantum chemical calculations have been performed in support of our experimental observations. Dimeric and trimeric alkali–metal–antimonides of the (Tip)<sub>2</sub>Sb<sup>–</sup> anion [M = Li, Na, K, Cs] have been isolated as dark-red solids from THF/toluene. The potassium analog of (Tip)<sub>2</sub>Sb<sup>–</sup> possesses a trimeric structure, while the other complexes [M = Li, Na, Cs] are dimeric both in the solid state and in solution. The electron transfer reduction processes of the reported complexes have been studied *via* CV measurements to rationalize the chemical synthesis. The dimeric Na antimonide (**15**) complex exhibits solvatochromism in solution. The trimeric K antimonide (**6**) is stable under an inert atmosphere for months at rt. The reactivity of [K<sub>3</sub>((Tip)<sub>2</sub>Sb)<sub>3</sub>(THF)<sub>5</sub>] (**6**) towards cAAC=P–Cl was explored. The reduction proceeds *via* a radical pathway. DFT calculations were in accordance with the experimental observations and we have attempted to provide a rationale for the proposed mechanism on the basis of free energy values. We believe that due to fundamental differences between antimony and phosphorous as elements, the former does not undergo reversible oxidation processes under ambient conditions like the latter and requires very high thermal energy to exist as a cationic species. Our studies showed that the redox-active (Tip)<sub>2</sub>Sb<sup>–</sup> anion can act as a reducing agent in THF. Furthermore, the (Tip)<sub>2</sub>Sb<sup>+</sup> cation can also be generated in solution. Finally, distibane (**4**) has been

studied *via* DFT/EDA-NOCV calculations to shed light on the unusual reduction of the Sb–Sb bond. The reduction properties of (Tip)<sub>2</sub>Sb<sup>−</sup> mean that it can be considered a new addition to the field of metal-complex-based reducing agents.<sup>44,45</sup>

## Conflicts of interest

There are no conflicts to declare.

## Acknowledgements

SR and KCM gratefully acknowledge SERB, New Delhi for their individual ECR grants (ECR/2016/000733 for SR; ECR/2016/000890 for KCM). EN thanks IISERT for SRF and AK thanks KYPY for financial support. MF and SMNVTG thank CSIR for their JRF and SRF, respectively.

## References

- (a) N. Zhang, S. R. Samanta, B. M. Rosen and V. Percec, Single Electron Transfer in Radical Ion and Radical-Mediated Organic, Materials and Polymer Synthesis, *Chem. Rev.*, 2014, **114**, 5848; (b) I. E. Scheffler, *Mitochondria*, Wiley, 2nd edn, 2007, ISBN: 978-0-470-04073-7.
- S. D. Minter, P. Christopher and S. Linic, Recent Developments in Nitrogen Reduction Catalysts: A Virtual Issue, *ACS Energy Lett.*, 2019, **4**, 163.
- P. W. Atkins, *Physical Chemistry*, Oxford University Press, Oxford, 6th edn, 1998, p. 830.
- J. R. Miller, L. T. Calcaterra and G. L. Closs, Intramolecular Long-Distance Electron Transfer in Radical Anions. The Effects of Free Energy and Solvent on the Reaction Rates, *J. Am. Chem. Soc.*, 1984, **106**, 3047.
- (a) P. Siders and R. A. Marcus, Quantum Effects in Electron-Transfer Reactions, *J. Am. Chem. Soc.*, 1981, **103**, 741; (b) P. Siders and R. A. Marcus, Quantum Effects for Electron-Transfer Reactions in the 'Inverted Region', *J. Am. Chem. Soc.*, 1981, **103**, 748; (c) R. A. Marcus, Electrostatic Free Energy and Other Properties of States Having Nonequilibrium Polarization, *J. Chem. Phys.*, 1956, **24**, 979.
- A. D. Clegg, N. V. Rees, O. V. Klymenko, B. A. Coles and R. G. Compton, Marcus Theory of Outer-Sphere Heterogeneous Electron Transfer Reactions: Dependence of the Standard Electrochemical Rate Constant on the Hydrodynamic Radius from High Precision Measurements of the Oxidation of Anthracene and Its Derivatives in Nonaqueous Solvents Using the High-Speed Channel Electrode, *J. Am. Chem. Soc.*, 2004, **126**, 6185.
- (a) W. R. Fawcett, The Role of the Metal and the Solvent in Simple Heterogeneous Electron Transfer Reactions, *Electrochim. Acta*, 1997, **42**, 833; (b) B. B. Smith and J. T. Hynes, Electronic Friction and Electron Transfer Rates at Metallic Electrodes, *J. Chem. Phys.*, 1993, **99**, 6517.
- G. A. Molander, Diverse Methods for Medium Ring Synthesis, *Acc. Chem. Res.*, 1998, **31**, 603.
- (a) M. I. Bruce, D. C. Kehoe, J. G. Matison, B. K. Nicholson, P. H. Rieger and M. L. Williams, Cluster Chemistry. Reactions between Metal Carbonyl Clusters and Lewis Bases Initiated by Radical Ions: Improved Syntheses of Substituted Derivatives of M<sub>3</sub> and M<sub>4</sub> Clusters (M = Fe, Ru, Os or Co), *J. Chem. Soc., Chem. Commun.*, 1982, 442; (b) N. G. Connelly and W. E. Geiger, Chemical Redox Agents for Organometallic Chemistry, *Chem. Rev.*, 1996, **96**, 877.
- (a) T. Kaese, A. Hübner, M. Bolte, H.-W. Lerner and M. Wagner, Forming B–B Bonds by the Controlled Reduction of a Tetraaryldiborane(6), *J. Am. Chem. Soc.*, 2016, **138**, 6224; (b) P. Lei, Y. Ding, X. Zhang, A. Adijiang, H. Li, Y. Ling and J. An, The Use of Bench-Stable Sodium Dispersions and Recoverable 15-Crown-5 Ether Enables a Significantly Improved, Practical, and Chemoselective Ammonia-Free Birch Reduction of a Broad Range of Aromatic and Heteroaromatic Compounds in Excellent yields, *Org. Lett.*, 2018, **20**, 3439; (c) C.-W. So, H. W. Roesky, P. M. Gurubasavaraj, R. B. Oswald, M. T. Gamer, P. G. Jones and S. Blaurock, Synthesis and Structures of Heteroleptic Silylenes, *J. Am. Chem. Soc.*, 2007, **129**, 12049.
- W. Wteurer, *Physical Metallurgy*, ed. R. W. Cahn and P. Haasen, 4th edn, 1996, Hardcover ISBN: 9780444898753.
- (a) Z.-H. Pan, J. Camacho, M. H. Upton, A. V. Fedorov, C. A. Howard, M. Ellerby and T. Valla, Electronic Structure of Superconducting KC<sub>8</sub> and Nonsuperconducting LiC<sub>6</sub> Graphite Intercalation Compounds: Evidence for a Graphene-Sheet-Driven Superconducting State, *Phys. Rev. Lett.*, 2011, **106**, 187002.
- (a) P. Vecera, J. Holzwarth, K. F. Edelthalhammer, U. Mundloch, H. Peterlik, F. Hauke and A. Hirsch, Solvent-Driven Electron Trapping and Mass Transport in Reduced Graphites to Access Perfect Graphene, *Nat. Commun.*, 2016, **7**, 12411; (b) A. Catheline, C. Vallé, C. Drummond, L. Ortolani, V. Morandi, M. Marcaccio, M. Iurlo, F. Paolucci and A. Pénicaud, Graphene Solutions, *Chem. Commun.*, 2011, **47**, 5470; (c) A. Catheline, L. Ortolani, V. Morandi, M. Melle-Franco, C. Drummond, C. Zakri and A. Pénicaud, Solutions of Fully Exfoliated Individual Graphene Flakes in Low Boiling Point Solvents, *Soft Matter*, 2012, **8**, 7882.
- T. A. Scott, B. A. Ooro, D. J. Collins, M. Shatruk, A. Yakovenko, K. R. Dunbar and H.-C. Zhou, After 118 Years, the Isolation of Two Common Radical Anion Reductants as Simple, Stable Solids, *Chem. Commun.*, 2009, 65.
- X.-L. Wu, R.-S. Wang, H. Yang, J. Zhang, M.-A. Fu, S.-C. Fang, X.-J. Chen, Y. Gao and Z.-B. Huang, Structural and Magnetic Properties of Potassium-Doped 2,3-Dimethylnaphthalene, *Crystals*, 2021, **11**, 608.
- (a) S. Roy, K. C. Mondal and H. W. Roesky, Cyclic Alkyl (amino) Carbene Stabilized Low Coordinate Metal Complexes of Enduring Nature, *Acc. Chem. Res.*, 2016, **49**,

- 357; (b) K. C. Mondal, S. Roy and H. W. Roesky, Silicon Based Radical, Radical ion and Diradical, *Chem. Soc. Rev.*, 2016, **45**, 1080; (c) M. Soleilhavoup and G. Bertrand, Cyclic (Alkyl)(Amino)Carbenes (CAACs): Stable Carbenes on the Rise, *Acc. Chem. Res.*, 2015, **48**, 256; (d) M. Arrowsmith, H. Braunschweig and T. E. Stennett, Formation and Reactivity of Electron-Precise B-B Single and Multiple Bonds, *Angew. Chem., Int. Ed.*, 2017, **56**, 96.
- 17 S. Roy, B. Dittrich, T. Mondal, D. Koley, A. C. Stückl, B. Schwederski, W. Kaim, M. John, S. K. Vasa, R. Linser and H. W. Roesky, Carbene Supported Dimer of Heavier Ketenimine Analogue with P and Si Atoms, *J. Am. Chem. Soc.*, 2015, **137**, 6180.
- 18 (a) A. E. Bragg, M. C. Cavanagh and B. J. Schwartz, Linear Response Breakdown in Solvation Dynamics Induced by Atomic Electron-Transfer Reactions, *Science*, 2008, **321**, 1817; (b) D. R. Widmer and B. J. Schwartz, Solvents can Control Solute Molecular Identity, *Nat. Chem.*, 2018, **10**, 910; (c) W. J. Glover, R. E. Larsen and B. J. Schwartz, Simulating the Formation of Sodium: Electron Tight-Contact Pairs: Watching the Solvation of Atoms in Liquids One Molecule at a Time, *J. Phys. Chem. A*, 2011, **115**, 5887.
- 19 S. Lin, L. Xu, A. C. Wang and Z. L. Wang, Quantifying Electron-Transfer in Liquid-Solid Contact Electrification and the Formation of Electric Double-Layer, *Nat. Commun.*, 2020, **11**, 399.
- 20 L. Yu, Q. Yan and A. Ruzsinszky, Key Role of Antibonding Electron Transfer in Bonding on Solid Surfaces, *Phys. Rev. Mater.*, 2019, **3**, 092801(R).
- 21 L. Lou and L. Österlund, Electronic Structure and Kinetics of K on Graphite, *J. Chem. Phys.*, 2002, **112**, 4788.
- 22 X. Zhao, S. A. Vail, Y. Lu, J. Song, W. Pan, D. R. Evans and J.-J. Lee, Antimony/Graphitic Carbon Composite Anode for High-Performance Sodium-Ion Batteries, *ACS Appl. Mater. Interfaces*, 2016, **8**, 13871.
- 23 C. Wu, L. Shen, S. Chen, Y. Jiang, P. Kopold, P. A. van Aken, J. Maier and Y. Yu, Top-Down Synthesis of Interconnected Two-Dimensional Carbon/Antimony Hybrids as Advanced Anodes for Sodium Storage, *Energy Storage Mater.*, 2018, **10**, 122.
- 24 (a) I. S. Ke, M. Myahkostupov, F. N. Castellano and F. P. Gabbaï, Stibonium Ions for the Fluorescence turn-on Sensing of F<sup>-</sup> in Drinking Water at Parts Per Million Concentrations, *J. Am. Chem. Soc.*, 2012, **134**, 15309; (b) A. Brückner, A. Hinz, J. B. Priebe, A. Schulz and A. Villinger, Cyclic Group 15 Radical Cations, *Angew. Chem., Int. Ed.*, 2015, **54**, 7426; (c) T. Li, H. Wei, Y. Fang, L. Wang, S. Chen, Z. Zhang, Y. Zhao, G. Tan and X. Wang, Elusive Antimony-Centered Radical Cations: Isolation, Characterization, Crystal Structures, and Reactivity Studies, *Angew. Chem., Int. Ed.*, 2016, **56**, 632; (d) M. M. Siddiqui, S. K. Sarkar, M. Nazish, M. Morganti, C. Köhler, J. Cai, L. Zhao, R. Herbst-Irmer, D. Stalke, G. Frenking and H. W. Roesky, Donor-Stabilized Antimony(I) and Bismuth (I) Ions: Heavier Valence Isoelectronic Analogues of Carbenes, *J. Am. Chem. Soc.*, 2021, **143**, 1301; (e) H. M. Weinert, C. Wölper, J. Haak, G. E. Cutsail and S. Schulz, *Chem. Sci.*, 2021, **12**, 14024.
- 25 M. Hirai and F. P. Gabbaï, Squeezing Fluoride out of Water with a Neutral Bidentate Antimony(V) Lewis Acid, *Angew. Chem., Int. Ed.*, 2015, **54**, 1205.
- 26 M. Hirai and F. P. Gabbaï, Lewis Acidic Stiborafluorenes for the Fluorescence turn-on Sensing of Fluoride in Drinking Water at ppm Concentrations, *Chem. Sci.*, 2014, **5**, 1886.
- 27 (a) X. Pan, Y. Su, X. Chen, Y. Zhao, Y. Li, J. Zuo and X. Wang, Stable Tetraaryldiphosphine Radical Cation and Dication, *J. Am. Chem. Soc.*, 2013, **135**, 5561; (b) T. Sasamori, E. Mieda, N. Nagahora, K. Sato, D. Shiomi, T. Takui, Y. Hosoi, Y. Furukawa, N. Takagi, S. Nagase and N. Tokitoh, One-Electron Reduction of Kinetically Stabilized Dipnictenes: Synthesis of Dipnictene Anion Radicals, *J. Am. Chem. Soc.*, 2006, **128**, 12582; (c) C. Helling and S. Schulz, Long-lived Radicals of the Heavier Group 15 Elements Arsenic, Antimony, and Bismuth, *Eur. J. Inorg. Chem.*, 2020, 3209; (d) C. Ganesamoorthy, C. Helling, C. Wölper, W. Frank, E. Bill, G. E. Cutsail and S. Schulz, From stable Sb- and Bi-centered radicals to a compound with a Ga=Sb double bond, *Nat. Commun.*, 2018, **9**, 87; (e) C. Helling, G. E. Cutsail III, H. Weinert, C. Wölper and S. Schulz, *Angew. Chem., Int. Ed.*, 2020, **59**, 7561.
- 28 S. Sasaki, F. Murakami, M. Murakami, M. Watanabe, K. Kato, K. Sutoh and M. Yoshifuji, Synthesis of Crowded Triarylphosphines Carrying Functional Sites, *J. Organomet. Chem.*, 2005, **690**, 2664.
- 29 H. J. Breunig, M. E. Ghesner and E. Lork, Syntheses of the Antimonides R<sub>2</sub>Sb<sup>-</sup> (R = Ph, Mes, <sup>t</sup>Bu, <sup>t</sup>Bu<sub>2</sub>(Sb) and Sb<sub>7</sub><sup>3-</sup> by Reactions of Organoantimony Hydrides or Cyclo-(<sup>t</sup>BuSb)<sub>4</sub> with Li, Na, K, or BuLi, *Z. Anorg. Allg. Chem.*, 2005, **631**, 851.
- 30 B = 6-311G\*\* (for C and H atoms) + Def2-TZVPP (for Sb and Cl atoms) + Def2-TZVPP Effective Core Potential for Sb atoms.
- 31 K. C. Mondal, S. Roy, B. Maity, D. Koley and H. W. Roesky, Estimation of  $\sigma$ -Donation and  $\pi$ -Backdonation of Cyclic Alkyl(Amino) Carbene-Containing Compounds, *Inorg. Chem.*, 2016, **55**, 163.
- 32 R. Kretschmer, D. A. Ruiz, C. E. Moore, A. L. Rheingold and G. Bertrand, One-, Two-, and Three-Electron Reduction of a Cyclic Alkyl(Amino)Carbene-SbCl<sub>3</sub> Adduct, *Angew. Chem., Int. Ed.*, 2014, **53**, 8176.
- 33 H. J. Breunig, I. Ghesner, M. E. Ghesner and E. Lork, Syntheses and Coordination Chemistry of Di-, Tri-, and Tetrastibanes, R<sub>2</sub>Sb(SbR')<sub>n</sub>SbR<sub>2</sub> (n = 0, 1, 2), *J. Organomet. Chem.*, 2003, **677**, 15.
- 34 R. Kretschmer, D. A. Ruiz, C. E. Moore, A. L. Rheingold and G. Bertrand, One-, Two-, and Three-Electron Reduction of a Cyclic Alkyl-(amino)carbene-SbCl<sub>3</sub> Adduct, *Angew. Chem., Int. Ed.*, 2014, **53**, 8176.
- 35 J. B. Waters, Q. Chen, T. A. Everitt and J. M. Goicoechea, N-Heterocyclic carbene adducts of the heavier group 15 tri-bromides. Normal to abnormal isomerism and bromide ion abstraction, *Dalton Trans.*, 2017, **46**, 12053.

- 36 J. E. Walley, L. S. Warring, E. Kertész, G. Wang, D. A. Dickie, Z. Benkó and R. J. Gilliard, Indirect Access to Carbene Adducts of Bismuth- and Antimony-Substituted Phosphaketene and Their Unusual Thermal Transformation to Dipnictines and  $[(\text{NHC})_2\text{OCP}][\text{OCP}]$ , *Inorg. Chem.*, 2021, **60**, 4733.
- 37 J. E. Walley, L. S. Warring, G. Wang, D. A. Dickie, S. Pan, G. Frenking and R. J. Gilliard, Carbodicarbene Bismaalkene Cations: Unravelling the Complexities of Carbene versus Carbene in Heavy Pnictogen Chemistry, *Angew. Chem.*, 2021, **133**, 6756.
- 38 See ref. 24c and d.
- 39 V. Kumar, R. G. Gonnade, C. B. Yildiz and M. Majumdar, Stabilization of the Elusive Antimony(I) Cation and Its Coordination Complexes with Transition Metals, *Angew. Chem., Int. Ed.*, 2021, **60**, 25522.
- 40 R. Deb, P. Balakrishna and M. Majumdar, Recent Developments in the Chemistry of Pn(I) (Pn = N, P, As, Sb, Bi) Cations, *Chem. – Asian J.*, 2022, **17**, e2021011.
- 41 O. Back, B. Donnadiou, P. Parameswaran, G. Frenking and G. Bertrand, Isolation of Crystalline Carbene-Stabilized P<sub>2</sub>-Radical Cations and P<sub>2</sub>-Dications, *Nat. Chem.*, 2010, **2**, 369.
- 42 G. Frenking, Multiple Bonding of Heavy Main-Group Atoms, in *The Chemical Bond: Chemical Bonding Across the Periodic Table*, ed. G. Frenking and S. Shaik, Wiley-VCH, Weinheim, 2014, p. 25.
- 43 D. J. D. Wilson, S. A. Couchman and J. L. Dutton, Are N-Heterocyclic Carbenes “Better” Ligands than Phosphines in Main Group Chemistry? A Theoretical Case Study of Ligand-Stabilized E<sub>2</sub> Molecules, L-E-E-L (L = NHC, phosphine; E = C, Si, Ge, Sn, Pb, N, P, As, Sb, Bi), *Inorg. Chem.*, 2012, **51**, 7657.
- 44 C. Jones, Dimeric Magnesium(I)  $\beta$ -Diketiminates: A New Class of Quasi-Universal Reducing Agent, *Nat. Rev. Chem.*, 2017, **1**, 1.
- 45 B. Rösch, T. X. Gentner, J. Eysel, J. Langer, H. Elsen and S. Harder, Strongly Reducing Magnesium(0) Complexes, *Nature*, 2021, **592**, 717.